2011

Modeling of Solar-Powered Single-Effect Absorption Cooling System and Supermarket Refrigeration/HVAC System

Ammar Bahman
University of South Florida, bo3mrh@gmail.com

Modeling of Solar-Powered Single-Effect Absorption Cooling System and Supermarket Refrigeration/HVAC System

by

Ammar Mohammad Khalil Bahman

A thesis submitted in partial fulfillment
of the requirements for the degree of
Master of Science in Mechanical Engineering
Department of Mechanical Engineering
College of Engineering
University of South Florida

Major Professor: Muhammad M. Rahman, Ph.D.
Luis Rosario, Ph.D.
Frank Pyrtle, III, Ph.D.
Craig Lusk, Ph.D.

Date of Approval:
June 13, 2011

Keywords: Lithium Bromide, COP, Cooling Capacity, Simulation, Display Cases, Energy Consumption, Store Relative Humidity

Dedication

To God, the Beneficent, the Merciful.

To my father, mother, brothers, and sisters,

for their great support during my graduate studies.

To my wife, Fatemah, for providing the lovely atmosphere for my study.

I dedicate this thesis especially to my beloved daughter, Laila.

Finally, to my Major Professor Muhammad Rahman,

for his immense patience and his enormous guidance.

Acknowledgements

I would like to express my sincere appreciation to Mutasim Elsheikh for his help and support through the complete of this thesis. I would like also to thank my colleague, Rashid Alshatti for his assistance and support during my study in the college.

Also, I would like to thank Professor Frank Pyrtle and Professor Craig Lusk for being my committee members. I really appreciate their constant support and help.

Special thanks to Dr. Luis Rosario and Dr. Jorge C. Lallave, for their guidance and valuable support.

Table of Contents

List of Tables

List of Figures

List of Symbols

A_C	Collector Area [m^2]
c_i	Correlated Constants i = 1-6 (Table 3.2)
CFD	Computational fluid dynamics
COP	Coefficient of performance
EER	Energy efficiency ratio
F_R	Collector heat removal factor
h	Enthalpy [kJ/kg]
HX	Heat exchanger
H_2O	Water
LV	Liquid-vapor
LLV	Liquid-liquid vapor
LiBr	Lithium bromide
m	Mass flow rate [kg/s]
$\dot{m}_a$	Air curtain mass flow rate [kg/s]
NP	Number of people
NRTL	Non-random two-liquid
P	Pressure [kPa]
q	Volume flow rate [m^3/s]
Q	Heat transfer [kW]

QL	Latent heat [kW]
R	Refrigerant
RH	Relative humidity [%]
S	Solar intensity [W/m^2]
T	Temperature [^{o}C]
U_L	Collector overall loss coefficient [W/m^2-K]
w	Humidity ratio

Greek Symbols

Δ	Deferential of change

Subscripts

a	Ambient
abs	Absorber
build	Supermarket building
con	Condenser
case	Display case
CI	Inlet of solar collector
evap	Evaporator
i	Process state number (i = 1, 2, 3, …etc)
infil	Infiltration
shx-c	Cold side of heat exchanger
shx-h	Hot side of heat exchanger
space	Supermarket space
S	Solar

Abstract

This thesis consists of two different research problems. In the first one, the aim is to model and simulate a solar-powered, single-effect, absorption refrigeration system using a flat-plate solar collector and LiBr-H_2O mixture as the working fluid. The cooling capacity and the coefficient of performance of the system are analyzed by varying all independent parameters, namely: evaporator pressure, condenser pressure, mass flow rate, LiBr concentration, and inlet generator temperature. The cooling performance of the system is compared with conventional vapor-compression systems for different refrigerants (R-134a, R-32, and R-22). The cooling performance is also assessed for a typical year in Tampa, Florida. Higher COP values are obtained for a lower LiBr concentration in the solution. The effects of evaporator and condenser pressures on the cooling capacity and cooling performance are found to be negligible. The LiBr-H_2O solution shows higher cooling performance compared to other mixtures under the same absorption cooling cycle conditions. For typical year in Tampa, Florida, the model shows a constant coefficient of performance of 0.94.

In the second problem, a numerical model is developed for a typical food retail store refrigeration/HVAC system to study the effects of indoor space conditions on supermarket energy consumption. Refrigerated display cases are normally rated at a store environment of 24ºC (75ºF) and a relative humidity of 55%. If the store can be maintained at lower relative humidity, significant quantities of refrigeration energy,

defrost energy and anti-sweat heater energy can be saved. The numerical simulation is performed for a typical day in a standard store for each month of the year using the climate data for Tampa, Florida. This results in a 24 hour variation in the store relative humidity. Using these calculated hourly values of relative humidity for a typical 24 hour day, the store relative humidity distribution is calculated for a full year. The annual average supermarket relative humidity is found to be 51.1%. It is shown that for a 5% reduction in store relative humidity that the display case refrigeration load is reduced by 9.25%, and that results in total store energy load reduction of 4.84%. The results show good agreement with available experimental data.

Chapter 1: Introduction and Literature Review

1.1 Introduction (Solar Absorption Cooling System)

The energy needed to process and circulate air in buildings and rooms to control humidity, temperature, and cleanliness has increased significantly during the last decade especially in developing countries. This energy demand has been caused by the increment of thermal loads to fulfill occupant comfort demands, climate changes, and architectural trends. The growth of electricity demand has increased especially at peak loads hours due to high use of driven vapor compression refrigeration machines for air conditioning. In addition, the consumption of fossil fuels and the emissions of greenhouse gases associated with electricity generation lead to considerable environmental consequences and monetary costs. Conventional energy resources will not be enough to meet the continuously increasing demand in the future. In this case, an alternative solution for this increasing demand of electrical power is solar radiation, available in most areas and representing an excellent supply of thermal energy from renewable energy resource.

One of the most common solar air conditioning alternatives is a solar powered absorption system. The solar absorption system is similar in certain aspect to the conventional vapor compression air conditioning system in that the electrical compressor; is replaced with a solar-powered generator and absorber. Figure 1.1 shows a commercial flat-plate solar-powered single-effect absorption cooling system. The most standard pairs

of chemical fluids used include lithium bromide-water solution ($LiBr-H_2O$), where water vapor is the refrigerant and lithium bromide is the absorbent, and ammonia-water solution (NH_3-H_2O) with ammonia as the refrigerant and water the absorbent [1]. The implementation of computer modeling of thermal systems offer a series of advantages by eliminating the cost of building prototypes, the optimization of the system components, estimation of thermal energy loads delivered or received from or into the system, and prediction of variations of the system parameters (e.g. temperature, pressure, mass flow rate).

Figure 1.1: Flat-plate solar-powered single-effect absorption cooling system.

1.2 Literature Review (Solar Absorption Cooling System)

A number of experimental and theoretical studies of solar-powered air-conditioning systems have been done in the past. Wilbur and Mitchell [2] compared theoretically single-stage, lithium bromide-water absorption cooling system heated from flat-plate solar collector to an ammonia-water system, and the lithium bromide system was preferred. It was shown that it required smaller cooling towers than the conventional one.

Li and Sumathy [3-4] experimentally studied a solar-powered absorption air conditioning system of lithium bromide-water solution as the refrigerant fluid. Their experimental results showed that using a partitioned hot-water storage tank is necessary to enhance the reliability of the system and achieve a continuous process operation.

Florides et al. [5] numerically studied a solar absorption cooling system with TRNSYS simulation program for the weather conditions of Nicosia, Cyprus. A system optimization was carried out in order to select the appropriate type of collector, the optimum size of the storage tank, collector slope and area under the two most favorable thermostats setting of the auxiliary boiler. The final optimized system consisted of a 15 m^2 compound parabolic solar collector tilted by 30^o from the horizontal and a $0.6m^3$ hot-water storage tank.

Atmaca and Yigit [6] developed a modular computer program for a solar-powered single-stage absorption cooling system using the lithium bromide-water solution as their working refrigerant. They examined various cycle configurations and solar energy parameters at Antalya, Turkey. The effects of hot water inlet temperatures on the coefficient of performance (COP) and the surface area of the absorption cooling

components were studied. The minimum allowable hot water inlet temperatures or reference temperature effects on the coefficient of performance were examined as part of their research. Their results showed that the increment of reference temperature decreases the absorber and solution heat exchanger surface area, and increases the system COP, while the size of the other components remains unchanged. Atmaca and Yigit [6] showed that evacuated, selective surface solar collector is the best option for the effective operation of their solar-power absorption cooling system. Their results showed that solar-power absorption cooling system requires a high performance collector.

Florides et al. [7] presented a method to evaluate the characteristics and performance of a single stage LiBr-water absorption machine. The heat and mass transfer equations including the appropriate equations of the working fluid properties were employed in a computer program as part of their research. The sensitivity analysis results showed that the greater difference between inlet and outlet concentrations of the LiBr-water solution at the absorber will reduce the mass flow rate. Florides et al. determined the cost for a domestic size absorber cooler, and concluded that despite the high price of the LiBr–water absorption cooling system in comparison with a electrical chiller of similar capacity, the absorption system remained favorable due to the use of renewable energy sources and waste heat, whereas the electric chiller uses electrical power that is produced from fossil fuels and has harmful effects on the environment. Assilzadeh et al. [8] studied a solar absorption cooling system that has been designed for Malaysia climate and similar tropical regions using TRNSYS numerical simulations. They used evacuated-tube solar collector for energy input to the absorption cooling system and Lithium bromide-water mixture as the working fluid. They proved that evacuated tube solar

collector provides high cooling performance at high temperature due to its high efficiency under this weather condition. The results showed that the cooling capacity of the system is large during periods of high solar radiation energy. The authors suggested a 0.8 m^3 hot-water storage tank in order to increase the reliability of the system and to achieve continuous operation for a 3.5 kW (1 refrigeration ton) system consists of 35 m^2 evacuated tubes solar collector sloped by 20^o as an optimum system at Malaysia's weather condition.

Mittal et al. [9] performed numerical simulations of a solar-powered single-stage absorption cooling system using a flat-plate solar collector and LiBr-water solution. A modular computer program was developed for the absorption system to simulate various cycle configurations with the help of weather data of Bahal village, district of Bhiwani on the western fringe of Haryana, India. The authors studied the effects of hot-water inlet temperatures on the coefficient of performance and the surface area of the absorption cooling component. Their results showed that the increment of the hot-water inlet temperature decreases the absorber and solution heat exchanger surface area, while the sizes of the other components remain the same. The authors examined the effect of reference temperature, the minimum allowable hot-water inlet temperature on the fraction of total load met by non-purchased energy (FNP), and the coefficient of performance. They concluded that high reference temperature increases the system COP and decreases the surface area of the system components; however, lower reference temperature shows better results for FNP. Sayegh [10] investigated an absorption cooling system powered with solar energy with the use of a thermal storage tank, auxiliary heater and flat plate solar collector for the weather conditions of Aleppo, Syria. Lithium bromide-water is

used as a working fluid for the system. A computational program is prepared to investigate the effect of varying the generator temperature between 80 to 100^{o}C, and the evaporator temperature between 5-15^{o}C on the coefficient of performance (COP) and solar useful heat gain of the absorption cooling system. Their results show that higher COP values are obtained by the increment of the generator temperature and the temperature drop of the evaporator. In addition, Sayegh [10] recommend the installation of seasonal thermal storage tank to decrease the AC load differences, which must be supplied by an auxiliary heater.

Balghouthi et al. [11] assessed the feasibility of solar-powered absorption cooling system under Tunisian weather conditions. They used TRNSYS and EES software's including a meteorological year data file containing the climatic condition of Tunis, the capital of Tunisia, in order to select and size the different components of the solar system to be installed. Their system was optimized for a typical building of 150m^2 and water lithium bromide absorption chiller with a capacity of 11 kW, and 30m^2 flat plate solar collector area tilted by 35^{o} from the horizontal and a 0.8m^3 hot-water storage tank. The simulation results showed that solar-power absorption cooling system is suitable under Tunisian conditions. The potential of integrated solar absorption cooling and heating systems for building applications were evaluated by Mateus and Oliveira [12]. The authors used TRNSYS software as a basis for their assessment. Different building types such as: residential, office and hotel and three different locations and climates from Berlin (Germany), Lisbon (Portugal), and Rome (Italy) were considered as part of their assessment. They ran the model for a whole year (365 days), according to control rules whether heating or cooling, and with the possibility of combining cooling, heating and

domestic hot water (DHW) applications. The different local costs for energy i.e. gas, electricity and water were taken into account for all cases. The authors concluded that residential house and hotel building types are the cases where the solar integrated system has a higher economic feasibility. For current energy costs, Rome was the only city to achieve a break-even situation. Their results showed a reduction in solar collector area between 15 to 50% by using vacuum tube collectors instead of flat-plate collectors. Conversely, flat-plate collectors lead to higher economic viability compared to vacuum tube collectors. To increase their marketability, integrated solar absorption cooling and heating systems need to reduce the initial costs of absorption chiller and solar collectors, considering the current costs of energy sources i.e gas and electricity. An optimization of solar collector size and other system parameters and CO_2 emissions savings were also assessed. An excellent reduction of CO_2 emissions were obtained by using an integrated solar system for combined heating and cooling in comparison with conventional systems. However, only a small number of papers could be found that considered a solar-powered cooling system using a flat-plate solar collector and LiBr-H_2O mixture as the working fluid.

The present study attempts to carry out a comprehensive investigation of a solar-powered single-effect absorption cooling system by using a flat-plate solar collector and LiBr-H_2O mixture as a working fluid. The modeling of the system components is carried out with the CHEMCAD software. Numerical computations were used to study the effect of inlet generator temperature on the cooling capacity and cooling performance of the system by varying different parameters (i.e. evaporator pressure, condenser pressure, mass flow rate, and LiBr-water solution concentration). The main contribution is to carry

out the cooling performance of solar-powered absorption cooling system by the comparison with a conventional vapor-compression system for different refrigerants. In addition, the cooling performance is also assessed for a typical year in Tampa, Florida.

1.3 Introduction (Supermarket Refrigeration/HVAC System)

Nowadays, the supermarket is a high-volume food sales outlet with maximum storage turnover. Most food products need to be kept under certain ambient temperature and relative humidity during operation hours. These foods are displayed in highly particular and flexible refrigerated display cabinets as shown in Figure 1.2. Most of the retail food can be spoiled unless refrigerated. These foods include meat, dairy products, frozen food, ice-cream and frozen desserts, and different individual items such as bakery and deli products and cooked meals. When a refrigerated display case operates in the supermarket environment, it exchanges heat and moisture within its environment. The moisture exchange between the display case and the store environment is the most troublesome part of this event due to an increase in energy requirement to maintain a satisfactory temperature within the display case. Nevertheless, maintaining a low relative humidity in the store environment requires an air-conditioning system with satisfactory performance characteristics. This maybe quite expensive with high operating cost. On the other hand, the operating cost of the display cases will be lower due to less latent load on the refrigeration coil, fewer defrosts to be required and less anti-sweat heater operation. Higher store relative humidity will result in lower operating cost of the air- conditioning equipment resulting in higher condensation on the display case walls, products and further frost on the evaporator coils.

(a)

(b)

(c)

Figure 1.2: Refrigerated display cases: (a) Vertical multi-shelf (b) Horizontal single-shelf (c) Closed door reach-in.

1.4 Literature Review (Supermarket Refrigeration/HVAC System)

In the literature, a reasonable number of research studies on refrigerated display cases have been reported. Howell and Adams [13] studied the effects of indoor space conditions on refrigerated display case performance. Howell [14, 15] developed a procedure that evaluates the effects of relative humidity on the energy performance of refrigerated display case energy requirement, anti-sweat heater energy, and defrost energy requirements. Howell [14] show that the savings in energy of the display cases ranged from 5% for closed door reach-ins cases to 29% for multi-shelf display cases when operated at store relative humidity of 35% rather than at 55%. The majority of the

cases saved 20% to 30% of their compressor energy, 40% to 60% in defrost energy, and 19% to 73% in anti-sweat heater operation for different types of display cases. The increment of AC energy requirement when the store operated at 35% relative humidity rather than 55%, ranged from 4% to 8% depending on the energy efficiency ratio (EER) value of the air-conditioning unit.

Tassou and Datta [16] investigated the effects of in-store environmental conditions on frost accumulation at the evaporator coils of open multi-deck refrigerated display cabinets. Their field and environmental chamber-based tests have shown that ambient relative humidity and temperature of a store have a significant effect on the rate of frost formation on the evaporator coils, with the effect of relative humidity being more evident than the effect of temperature. They concluded that a considerable opportunity exists to implement sophisticated defrost control strategies to save energy and improve temperature control. Orphelin et al. [17] discussed a new approach to estimate impacts of temperature and humidity set points on the total energy balance of typical French supermarkets. Their model took into account the cold aisle effect and the occurrence of thermal coupling between the supermarket display cases and the air-conditioning system. Their results showed that it is not cost effective to maintain a lower relative humidity level under 40% within the store during summer time. In addition, their results showed that the performance of air-conditioning and refrigeration systems of the operating the display cases, have to be well known in order to define an acceptable set point in terms of energy consumption and customer comfort.

Rosario and Howell [18] experimentally evaluated the energy savings produced by reducing the relative humidity of the store. Eight supermarkets in the Tampa, Florida

area were monitored for twelve hours and seven day periods between November 1997 and October 1998 in order to know the typical store relative humidity prior to its potential reduction. Five different areas of the eight supermarkets were monitored. The relative humidity within the store differed up to 20% and the average annual relative humidity between different stores varied up to 12%. Their results show that the average relative humidity of all stores have a minimum value of 37% during the month of March and a maximum value of 56% during the month of September. The annual average value for all stores is 45%. An algebraic expression based on experimental results was used to correlate indoor humidity ratio as a function of outdoor humidity ratio. Their results showed that the theoretical moisture balance model's prediction was within ±10% in comparison with the experimental data. They concluded that the total store energy bill (i.e. display cases, air-conditioning and lights) could be reduced up to 5% by lowering the store relative humidity by 5%. The store relative humidity reduction of 1% represented the savings of 18,000 to 20,000 kWh annually.

Kosar and Dumitrescu [19] provided an updated review of currently available databases that address the effect of supermarket humidity on refrigerated case energy performance from computer simulations, laboratory tests, and field evaluations. Their database reviewed findings and tabulated those by case type, humidity range, and energy performance impact which were separated by compressor energy, defrost energy, and anti-sweat energy. Their findings revealed that the reduction in anti-sweat energy heater operation, compressor energy reductions, and electrical defrost reductions represent the 55%, 44%, and 1% of the store energy savings potential respectively. Although these conclusions differ with the store mix of case types and controls for anti-sweat and defrost

operation, it is clear that anti-sweat heater requirements deserve as much attention as compressor or refrigeration loads of display cases at low humidity levels.

Chen and Yuan [20] experimentally invistegated the effects of some important factors on performance of a multi-shelf refrigerated display case. The factors include the ambient temperature and humidity, discharge air velocity, night covers and air flow from perforated back panels. Both inside and temperature distribution and cooling were studied. The results showed that ambient temperature and relative humidity increse causing the temperature and heat gain of the display case to increase. In addition, the results were in great significance to the optimum design of display cases and energy management of supermarkets.

Due to the importance of numerical modelling to have effective and effiecient refrigerated systems, Smale et al. [21] reviewed all numerical modelling techniques and the application of CFD during the period of 1974 to 2005 for the prediction of airflow in refrigerated food applications including cool stores, transport equipments, and retail display cabinets.

Getsu and Bansal [22] numerically and experimentally analysed evaporator in frozen food display cases at low temperature in the supermarket in Auckland, New Zealand. Extensive experiments were conducted to measure store and display case relative humidities and temperatures, and pressures, temperatures and mass flow rates of refrigerants. The mathematical model used different empirical correlations of heat transfer coefficient and frost properties for the heat exchanger in order to investigate the influence of indoor conditions on the performance of the display cases. Experimental data were used to validate the model so that the model would be a tool for designers to

evaluate the performance of supermarket display case heat exchangers under different retail store conditions.

Ge et al. [23] integrated CFD with cooling coil model to simulate and analyse the performance of multi-deck medium temperature display case. The 2D CFD model can predict the air dynamics of air flow, heat and mass transfer among the air flow, food products and ambient space air. The model simulated different pipe and fin structures and circuit arrangements, with the outputs from the cooling coil model used as the inputs to the CFD model and vice versa. A typical multi-deck medium temperature display case was selected as a prototype and mounted into an air conditioned chamber to validate this integrated model. The validated model was used to examine the cabinet performance and explore the optimal control strategies at various operating conditions and design conditions.

The importance of an air curtain in refrigerated display cases modeling motivated many researches and a number of studies have been published on the development of an air curtain. Howell et al. [24] theoretically and experimentally investigated the heat and moisture transfer through turbulent plane air curtains. They investigated the performance of air curtain by the variation of the number of jets, thickness, width, height, velocity, turbulence level of the air curtain, and pressure and temperature difference across the air curtain. An eddy viscosity model was used with finite difference technique to calculate the sensible, latent, and total heat transfer through air curtains. Their results showed that the total heat transfer is directly proportional to the initial velocity and the temperature difference across the air curtain, including the significant effect of the initial turbulence

intensity that could reach up to 32% increment of heat and moisture transfer through an air curtain.

Howell and Shibata [25] experimentally investigated the relationship between the heat transfer through a recirculated air curtain and its deflection modulus. The deflection modulus was defined as the ratio of the initial momentum of the air curtain jet and the transverse forces magnitude in which the air curtain attempts to seal against. Their research investigated the performance of air curtain by the variation of the number of jets, thickness, width, height, velocity, turbulence level of the air curtain, and pressure and temperature difference across the door opening. The authors demonstrated that there is an optimum flow velocity for the air curtain to seal the doorway and minimize the heat transfer rate and moisture effect. Their findings show that transverse and longitudinal temperature differences can be used as one of the correlating parameters of recirculated air curtains, including the value of the deflection modulus which exists for each air curtain configuration which minimizes the heat transfer rate across the air curtain.

Ge and Tassou [26] developed a comprehensive model, based on the finite difference technique, which can be used to predict and optimize the performance of air curtains. Based on the results obtained from their model, correlations for the heat transfer across refrigerated display case air curtains have been developed to enable quick calculations and parametric analyses for design and refrigeration equipment sizing purposes. In this study, the authors have shown that both the finite difference and simplified models can be used to determine the total cooling load of vertical refrigerated display cases with a reasonable degree of accuracy.

Cui and Wang [27] used a computational fluid dynamics (CFD) method to evaluate the energy performance of an air curtain for horizontal refrigerated display cases and optimize their design. The CFD method was validated by comparing the CFD calculations with experimental results. The authors studied the key factors that influence the air curtain cooling load such as: air curtain velocity, the height and shape of products inside the display case, temperature difference between the inlet and ambient air, and the relative humidity of the ambient. Their results showed that there is an optimum value for the inlet velocity of the air curtain, while other design parameters remain unchanged. They also found that the air curtain is heavily affected by both the inlet air temperature and the relative humidity of ambient air. The larger the temperature difference and/or relative humidity difference between the inlet and ambient air, the more intensive will be the heat and mass transfer between the air curtain and the ambient air. Therefore, properly controlled indoor conditions, i.e. dry-bulb temperature and relative humidity, could well balance the cooling load of the store against that of the display cases and help achieve overall energy efficiency. Cui and Wang [27] concluded that the CFD method is an effective and feasible tool for the optimal design and performance evaluation of air curtain of horizontal refrigerated display cases.

Navaz et al. [28] presented a comprehensive discussion on past, present, and future research focused on display case air curtain performance characterization and optimization. Ge and Cropper [29] developed a display case model by the integrating three main component sub-models, an air-cooling finned-tube evaporator, an air curtain and a display case body at steady state. In their work, they described the analysis and performance comparison of a display cabinet system using R404A and R22 as the

refrigerants. They concluded that the total cooling load of display case and refrigerant mass flow rate increased at higher ambient air humidity. In addition, the increment of ambient air humidity will affect significantly the latent cooling load more than its sensible load. The increment of cooling load or refrigerant mass flow rate of the R404A refrigerant increased the power consumption of the refrigeration unit. At a specified operating condition, R404A refrigerant display case required greater cooling loads and refrigerant mass flow rates than R22 refrigerant units.

The objective of this work is to model a supermarket refrigeration/HVAC system, and to develop a numerical simulation for this model using MATLAB. The model is integrating the air curtain model developed by [26] for display cases within the main supermarket model. The simulation is performed for a typical day under standard store conditions for each month of the year using climate data for Tampa, Florida. A parametric study of this system and a prediction of energy consumption are done to study the effect of indoor space conditions on supermarket energy consumption. A sensitivity analysis is performed for the proposed model and validated with available experimental data. The main contributions are to validate the air curtain model developed by [26] within the supermarket model for Tampa, Florida weather conditions and calculate the energy consumption when the store relative humidity is reduced.

Chapter 2: Solar-Powered Single-Effect Absorption Cooling System

2.1 System Description

The solar-powered absorption cycle consists of four major parts, i.e., a generator, a condenser, an evaporator and an absorber. These major components are divided into three parts by one heat exchanger, two expansion valves and a pump. Schematic diagrams of the solar-powered cooling system are shown in Figures 2.1 and 2.2. Initially, the collector receives energy from sunlight and heat is accumulated in the storage tank. Subsequently, the energy is transferred through the high temperature energy storage tank to the refrigeration system. The solar collector heat is used to separate the water vapor, stream number 2, from the lithium bromide solution, stream number 3, in the generator at high temperature and pressure resulting in higher lithium bromide solution concentration. Then, the water vapor passes to the condenser where heat is removed and the vapor cools down to form a liquid, stream number 4. The liquid water at high pressure, stream number 4, is passed through the expansion valve, stream number 9, to the evaporator, where it gets evaporated at low pressure, thereby providing cooling to the space to be cooled. Subsequently, the water vapor, stream number 5, goes from the evaporator to the absorber. Meanwhile, the strong lithium bromide solution, stream number 3, leaving the generator for the absorber passes through a heat exchanger in order to preheat the weak solution entering the generator, and then expanded to the absorber, stream number 6. In the absorber, the strong lithium bromide solution absorbs the water vapor leaving the

evaporator to form a weak solution, stream number 7. The weak solution, stream number 8, is then pumped into the generator and the process is repeated.

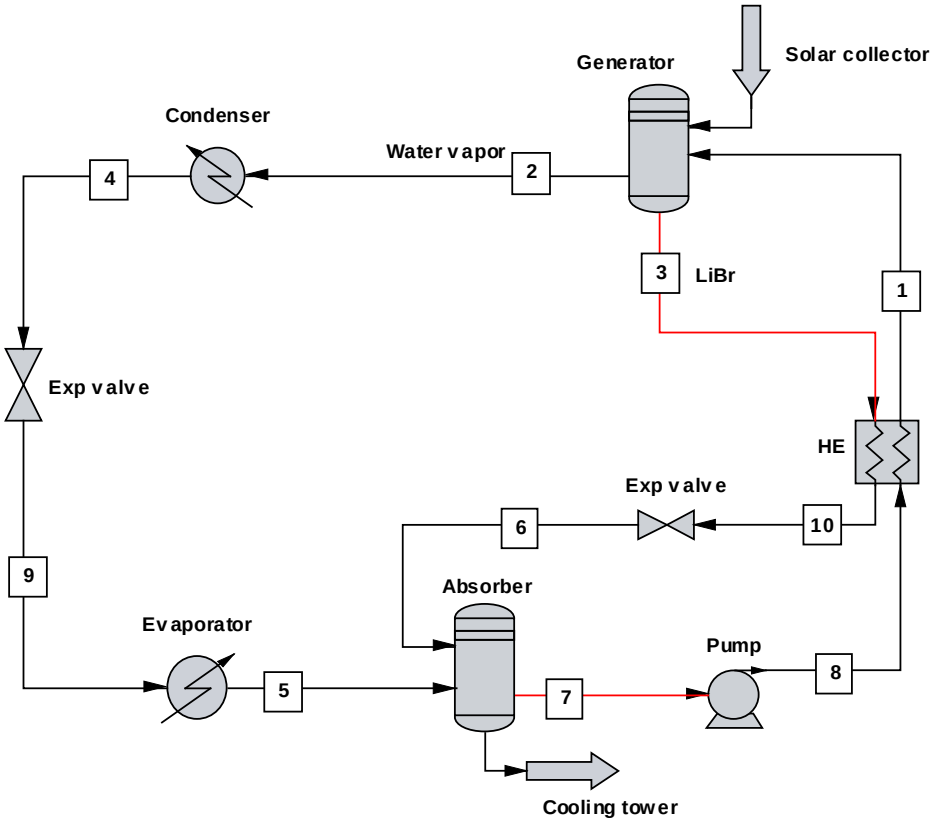

Figure 2.1: Schematic diagram of the absorption cycle.

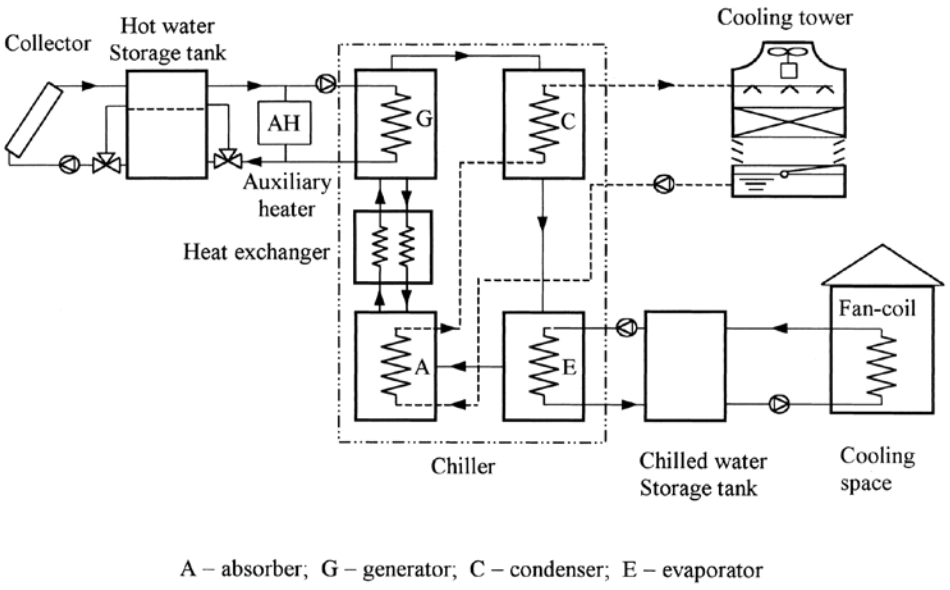

Figure 2.2: Schematic diagram of the solar-powered air conditioning system [1].

Generally, the heat is removed from the system by a cooling tower. The cooling water passes through the absorber first then the condenser. The temperature of the absorber has a higher influence on the system efficiency than the condensing temperature of the cooling tower where the heat is dissipated to the environment. In the case that the sun is not shining, an auxiliary heat source is used by electricity or conventional boiler to heat the water to the required generator temperature. It is highly recommended to use a partitioned hot-water storage tank to serve as two separate tanks. In the morning, the collector system is connected to the upper part of the tank, whereas in the afternoon, the whole tank would be used to provide heat energy to the system.

2.2 Mathematical Model

A control volume is taken across each component i.e. the generator, absorber, evaporator, condenser and heat exchanger to analyze the working conditions of all components of the system. The mass and the energy balances are performed and a computer simulation is developed for the cycle analysis. A control volume analysis around each component, which covered the rate of heat addition in the generator, and the energy input of the cycle, is given by the following equation:

$$Q_{gen} = h_2 m_2 + h_3 m_3 - h_1 m_1 \quad (1)$$

The rate of heat rejection out of the condenser is given by the following equation:

$$Q_{con} = m_2 (h_2 - h_4) \quad (2)$$

The rate of heat absorption of the evaporator is given by the following equation:

$$Q_{evap} = m_2 (h_5 - h_9) \quad (3)$$

The rate of heat rejection of the absorber is given by the following equation:

$$Q_{abs} = h_5 m_2 + h_6 m_3 - h_7 m_1 \quad (4)$$

An energy balance on the hot side of the heat exchanger is given by the following equation:

$$Q_{shx-h} = m_3 (h_3 - h_{10}) \quad (5)$$

Similarly an energy balance on the cold side of the heat exchanger is given by the following equation:

$$Q_{shx-c} = m_1 (h_1 - h_8) \quad (6)$$

The overall energy balance on the heat exchanger is satisfied if $Q_{shx-h} = Q_{shx-c}$ which is valid in this case.

Coefficient of performance (COP) according to Figure 2.1 is defined as follows:

$$COP = \frac{Q_{evap}}{Q_{gen}} \tag{7}$$

The solar collector was modeled in the manner proposed by Klein, Duffie, and Beckman [30]. The basic equation for flat-plate solar collector is given by:

$$Q_S = F_R A_C [S - U_L (T_{CI} - T_a)] \tag{8}$$

For simplicity, the collector heat removal factor of F_R = 0.8 is used. Average solar intensity is shown in Figure 2.3 for typical year in Tampa, Florida [31]. The average flat-plate solar collector loss coefficient of U_L = 3.0 W/m^2-K is held constant. The collector inlet temperature T_{CI}, and the ambient temperature T_a are assumed to be 80^{o}C and 30^{o}C, respectively.

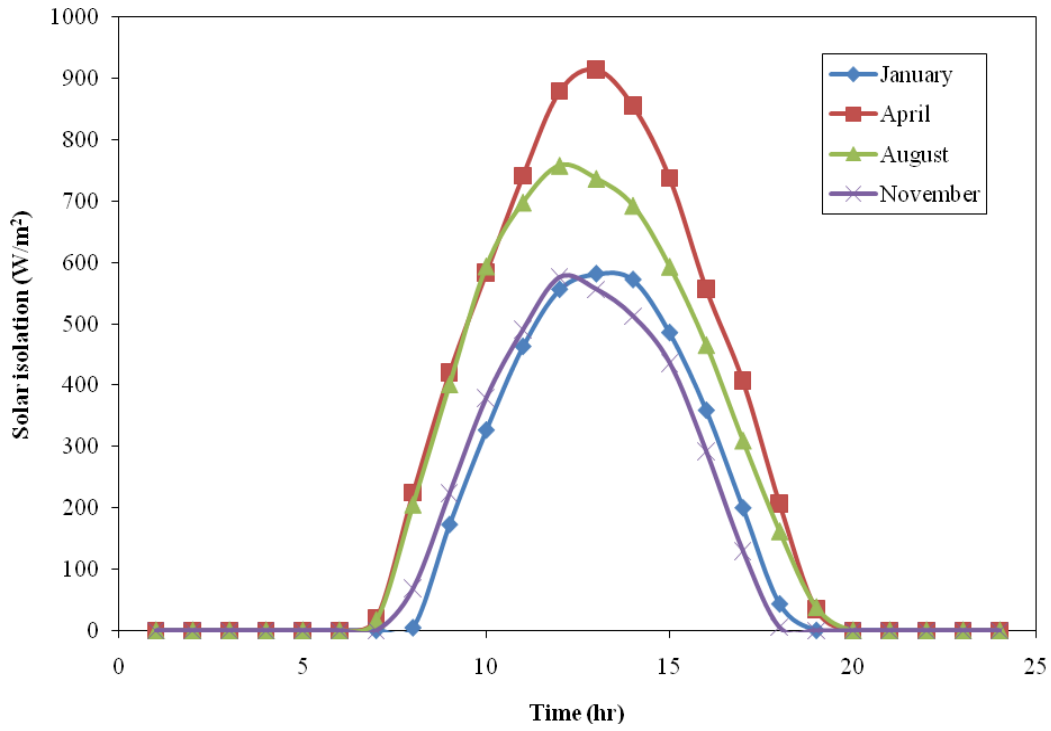

Figure 2.3: Hourly solar isolation for Tampa, Florida [31].

2.3 Model Simulation

CHEMCAD [32] was used to simulate the solar-powered lithium bromide absorption system. The generator and absorber were modeled by using a multipurpose flash column. CHEMCAD uses the flash column to visualize generator and absorber operations. Simultaneously, a modular mode was used to solve the algebraic equations of the flow sheet. The Non-random two-liquid (NRTL) model and latent-heat enthalpy model were used in the simulation to obtain the thermodynamic properties and phase equilibrium of the Lithium bromide solution. The NRTL model software keeps all flashes as three-phase flashes (LLV) or two-phase flashes (LV). Liquid phase activity coefficients are calculated by the NRTL equation by the known values of the liquid phase mass fraction. The NRTL equation is a good method to solve the binary mixture where equilibrium prevails between liquid and vapor [33]. Previous studies have shown that the NRTL equation is in good agreement with the experimental phase equilibrium of Lithium bromide solution [34]. The simulation model was also compared with a solar absorption air conditioning study which was carried out in Tunisia using TRNSYS and EES programs [11]. The following parameters and assumptions were used in the simulation:

Strong solution concentration of 0.561 (LiBr mass fraction);

Strong solution mass flow rate m_1 = 0.056 kg/s;

The water vapor mass flow rate m_2 = 0.0048 kg/s;

The high and low pressures of the system were set at 6.601 and 0.9 kPa, respectively;

Generator heat duty Q_{gen} = 15.26 kW;

Pressure drops were neglected;

Work input by the pump was neglected.

The comparison of present numerical results and Balghouthi et al. [11] results are shown in Table 1 and 2. The numerical data obtained are in good agreement with Balghouthi et al. [11] results.

Table 2.1: Operation condition (a) [11], (b) CHEMCAD process model.

Stream	*T* (^{o}C)		*P* (kPa)		x (kg LiBr/kg solution)		*m* (kg/s)	
	(a)	(b)	(a)	(b)	(a)	(b)	(a)	(b)
1. Pump outlet	36.2	36.2	6.601	6.601	0.561	0.561	0.056	0.056
2. Condenser inlet	70	71.2	6.601	6.601	0	0	0.0048	0.0048
3. Generator outlet	84.6	71.2	6.601	6.601	0.613	0.614	0.0512	0.0512
4. Condenser outlet to exp. valve	38	37.8	6.601	6.601	0	0	0.0048	0.0048
5. Vapor from evaporator to absorber	4.4	5.4	0.9	0.9	0	0	0.0048	0.0048
6. Solution inlet in absorber	47.1	31.3	0.9	0.9	0.613	0.614	0.0512	0.0512
7. Absorber outlet	36.2	36.2	0.9	0.9	0.561	0.561	0.056	0.056
8. Generator inlet from heat exchanger	62.4	62.4	6.601	6.601	0.556	0.561	0.056	0.056
9. Evaporator inlet from expansion valve	5.5	5.4	0.9	0.9	0	0	0.0048	0.0048
10. Absorber inlet from heat exchanger	53.6	69.3	6.601	6.601	0.613	0.614	0.0512	0.0512
11. Generator inlet from heat exchanger	62.4	62.4	6.601	6.601	0.556	0.561	0.056	0.056

Table 2.2: Energy flow at various component of the system (a) [11], (b) CHEMCAD process model.

Description	Symbol	Energy (kW)	
		(a)	(b)
Evaporator	Q_{evap}	11.31	11.26
Absorber	Q_{abs}	14.67	14.61
Generator	Q_{gen}	15.26	15.26
Condenser	Q_{con}	11.89	11.90
Coefficient of performance	COP	0.74	0.74

The input data required for simulating the system consists of the following: generator temperature, absorber temperature, generator and condenser pressure, evaporator and absorber pressure, pump output pressure, mass flow rate entering generator, lithium bromide solution concentration entering the generator and fixed saturated liquid state from heat exchanger to generator. Figure 2.4 shows flow-diagram for how simulation works using input data. The output includes the generator heat gain, cooling capacity and COP.

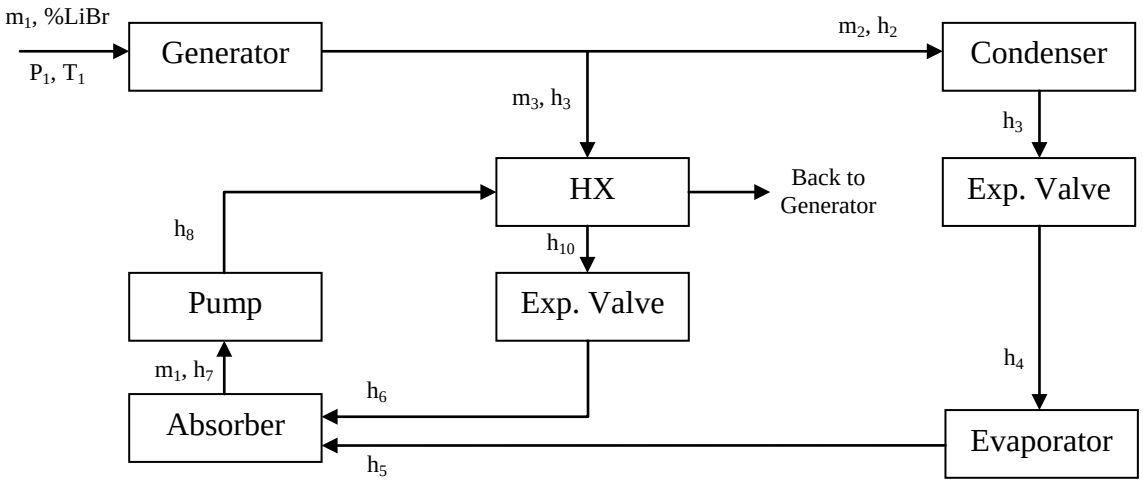

Figure 2.4: Information-flow diagram for solar-powered absorption cooling system.

2.4 Results and Discussion

Simulation results are presented here for the performance of the solar-powered absorption cooling system. The effect of the variation of the inlet generator heating water temperature is shown in figure 2.5. The cooling capacity varies approximately linearly starting from a low value of 0.47 kW up to 16 kW. The COP rises from a low value of 0.82 to reach a constant value of 0.94. The cooling capacity increases as the inlet generator temperature increases. The COP of the system increases slightly when the heat source temperature increases.

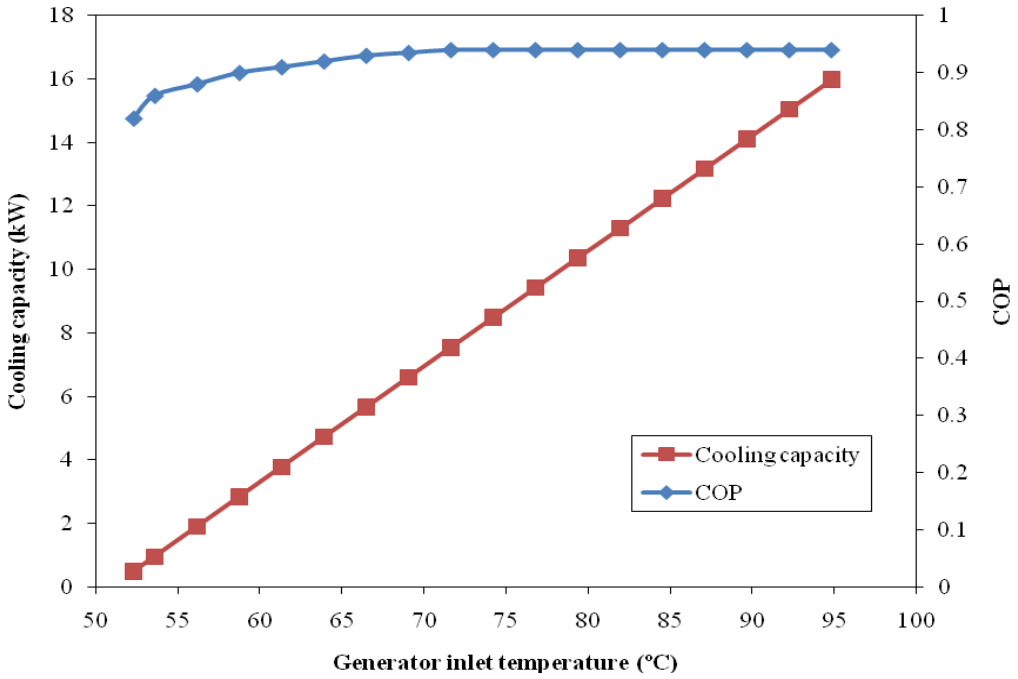

Figure 2.5: Effect of generator inlet temperature on cooling capacity and COP.

The COP would be expected to increase significantly with increasing generator/source temperature, but as the generator/source temperature increases, the heat transfer in all the heat exchangers of the system also increases as shown in Figure 2.6.

The figure shows linear increase in the heat transfer in all of evaporator, condenser and absorber when varying the inlet generator temperature.

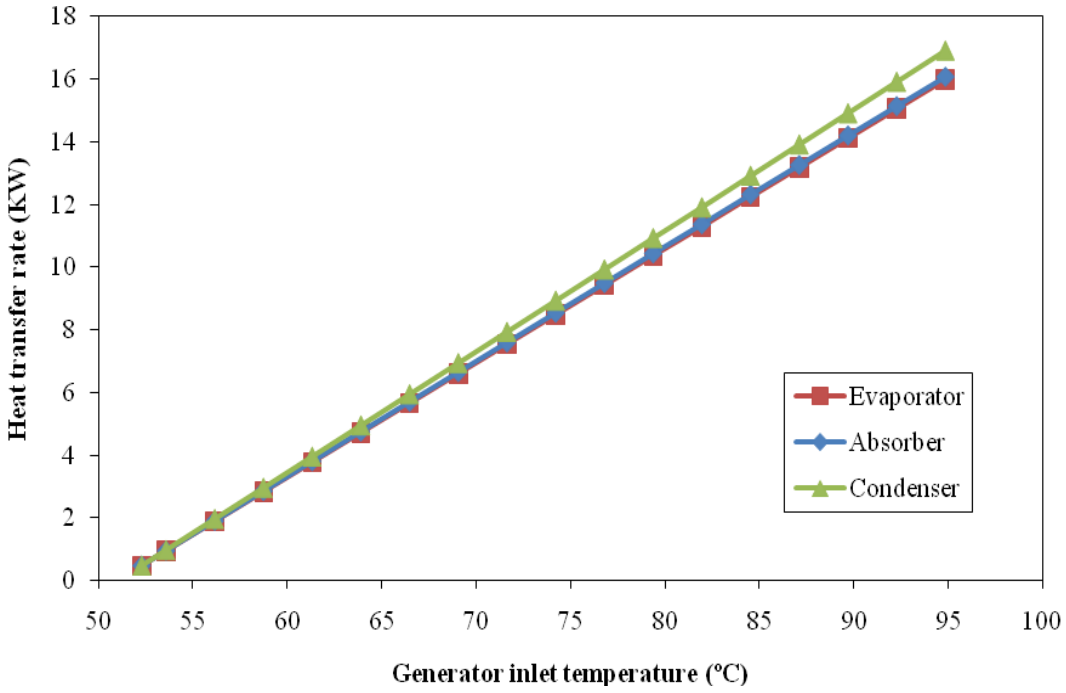

Figure 2.6: Effect of generator inlet temperature on evaporator, absorber, condenser and generator heat transfer rates.

Figure 2.7 shows that the evaporator temperature decreases with the source temperature while the generator outlet solution temperature and the condensation temperature increase. The generator inlet temperature could not be increased or decreased too much because of the crystallization of the lithium bromide. Because lithium bromide is a salt, in its solid state it has a crystalline structure. There is a specific minimum solution temperature for any given salt concentration when lithium bromide is dissolved in water. The salt begins to leave the solution and crystallize below this minimum temperature. In an absorption system, if the LiBr-solution concentration is too high or if

the LiBr-solution temperature is reduced too low, crystallization may occur [7]. The crystallization influences the cycle performance and the temperatures at different streams. There are several causes for crystallization. Air leakage into the system is one of most common reason for crystallization. Air leakage results in increased pressure in the evaporator. This, in turn, results in higher evaporator temperatures and, consequently, lower cooling capacities. In the other case, at high load conditions, the control system increases the heat input to the generator, resulting in increased solution concentrations to the level where crystallization may occur. Non-absorbable gases, like hydrogen, produced during corrosion, can also be present, this can reduce the performance of both the condenser and the absorber. Electric power failure is found to be another reason for crystallization [7]. Crystallization is most likely to occur when the machine is stopped while operating at full load, when highly concentrated solutions are present in the solution heat exchanger. To solve this problem, during normal shutdown, the system should go into a dilution cycle, which lowers the concentration of the LiBr-solution throughout the system, so that the machine may cool to ambient temperature without crystallization occurring in the solutions.

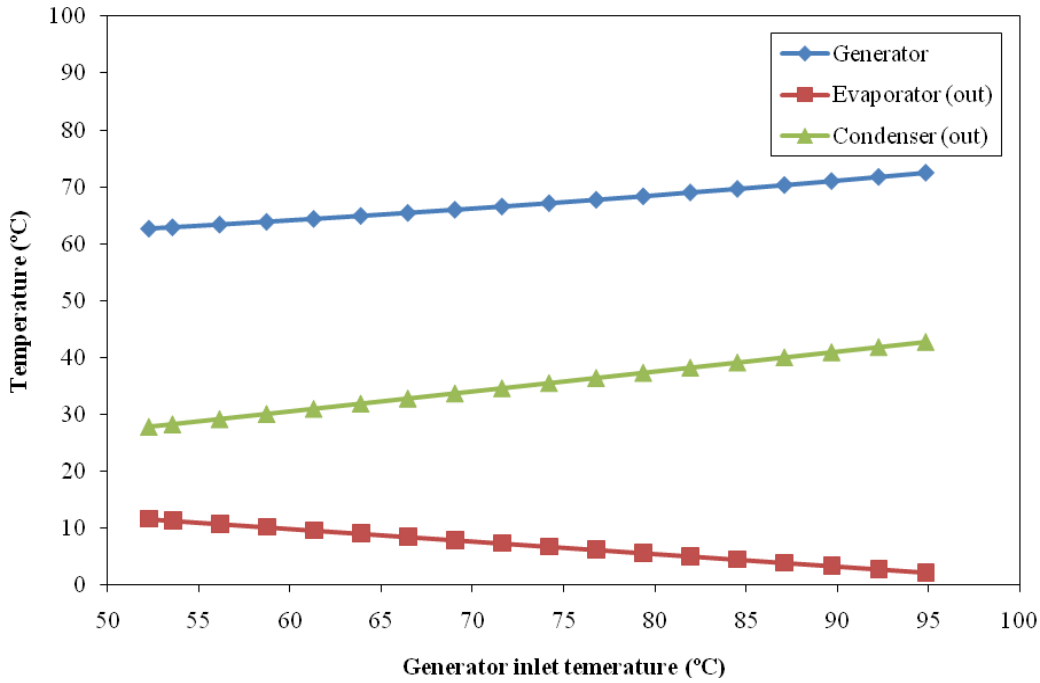

Figure 2.7: Effect of generator inlet temperature on generator, evaporator and condenser temperatures.

Figure 2.8 shows the generator heat gain when increasing the collector area using Klein, Duffie and Beckman equation [30]. The greater the collector area the greater the heat gained. This can be good for the auxiliary boiler. Once the heat gained is increased, less heat is required from the auxiliary boiler to maintain the required generator temperature.

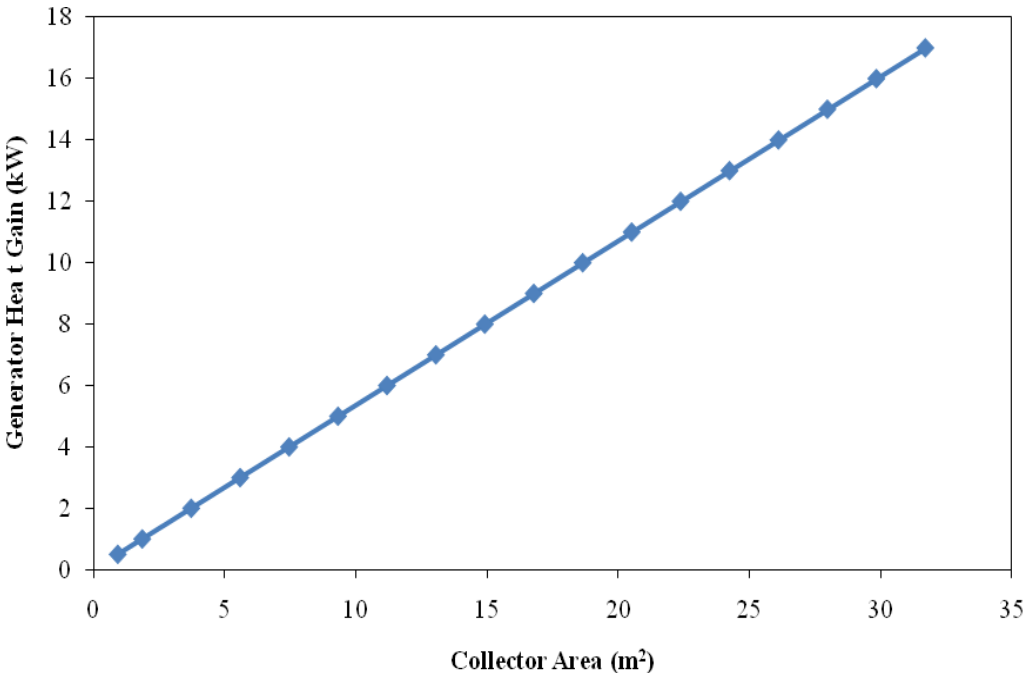

Figure 2.8: Effect of the collector area on the heat gain using Klein, Duffie, and Beckman equation.

Figure 2.9 illustrates comparison of cooling load and coefficient of performance for both CHEMCAD model and TRNSYS model [11]. The current model shows matching trends with the previous study of [11]. Increasing the heat source temperature increases the cooling capacities linearly for both models. The COP for both models has the same trend. For temperatures less than 70^{o}C, the COP increases slightly. As the generator inlet temperature increases, the COP reaches constant values of 0.75 and 0.72 for both CHEMCAD and TRNSYS models, respectively. The reason for this discrepancy is due to different equations of state used in the softwares; NRTL was used in CHEMCAD and nonlinear equation solver was used in TRNSYS. Also, for simplicity, the overall heat transfer coefficients for all major components are assumed to be negligible in the current model, this, in turn, results in higher cooling load and lower heat in the generator and so on higher COP.

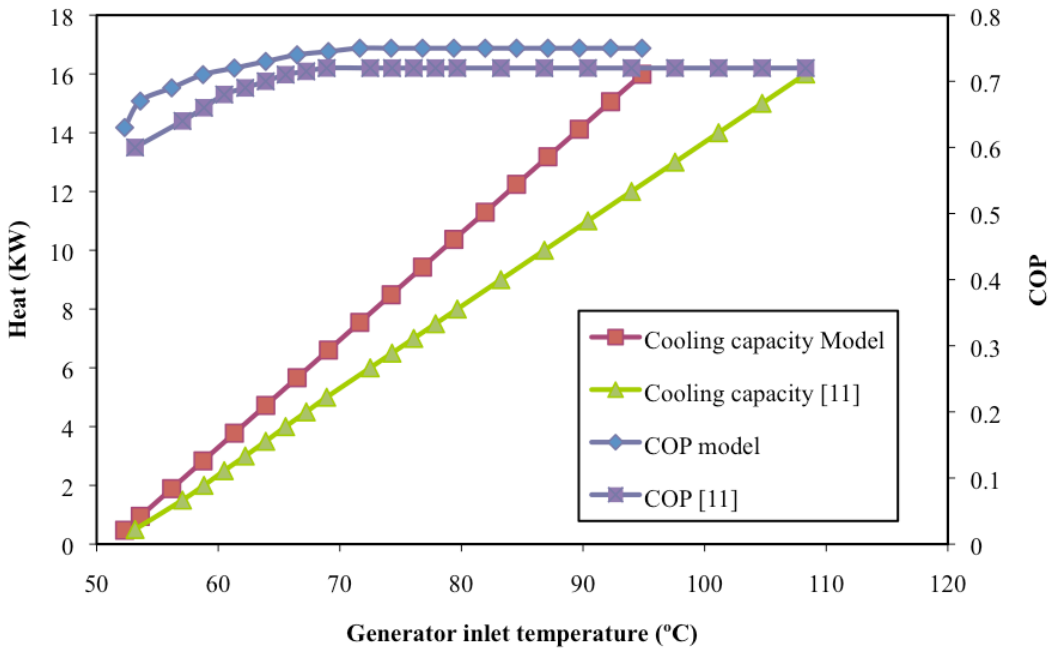

Figure 2.9: Comparison of cooling load and COP for CHEMCAD model and [11].

The change of the cooling performance (COP) of refrigerants for different cooling cycles is reported in Table 2.3. Özkan et al. [35] compared the performance of different refrigerants like R-600a, R-134a, R-290, R-1270, R-32, R-22, and R-152a in vapor compression refrigeration cycle. He et al. [36] examined the efficiency characteristics of R-22+DMF, R-134a+DMF and R-32+DMF in solar-powered absorption cooling system. Table 2.3 compares the COP for [35] and [36] with the current study. A cooling load of 2.2 kW was used as a reference to compare between the refrigerants. According to the table, the COP of R-22 is the highest while the COP of R-32+DMF is the lowest. Refrigerants R-134a, R-32 and R-22 have COP values larger than one. In the other hand, the mixtures Libr-H_2O, R-22+DMF, R-134a+DMF and R-32+DMF have COP values less than one. Both the refrigerant and refrigeration cycle influence the value of COP. It is well known that the vapor compression refrigeration cycles have COP value larger than

one, while the solar-powered absorption systems have COP value less than one [37]. This is due to the different definition for the COP for the vapor compression system and the absorption system. If the COP definition of vapor compression cycle was used to find the COP of the solar absorption cycle, the COP of the solar absorption cycle would have very high COP, around 1000 times the value of 0.88, because of the low required input works in such systems. Despite the low COP of the solar-powered absorption systems, it can help in reducing the use of fossil fuel. The table shows that LiBr-H_2O mixture used in solar-powered absorption cooling system has COP value higher than refrigerant-DMF solutions used in the same solar-powered absorption cooling system. For solar-powered absorption cooling system with COP higher than one, it is required to have double-effect or triple-effect systems to operate with COP higher than one [37-38]. Figure 2.10 and 2.11 show schematic diagrams for double-effect and triple-effect absorption refrigeration systems, respectively. Notice that there are additional generators and heat exchangers used for multi-effect absorption systems.

Table 2.3: Comparison of COP for different refrigerants for different cooling cycles with cooling capacity of 2.2 kW.

Refrigerant	COP
R-134a	1.9
R-32	1.9
R-22	1.99
LiBr-H_2O	0.88
R-22+DMF	0.3
R-134a+DMF	0.5
R-32+DMF	0.1

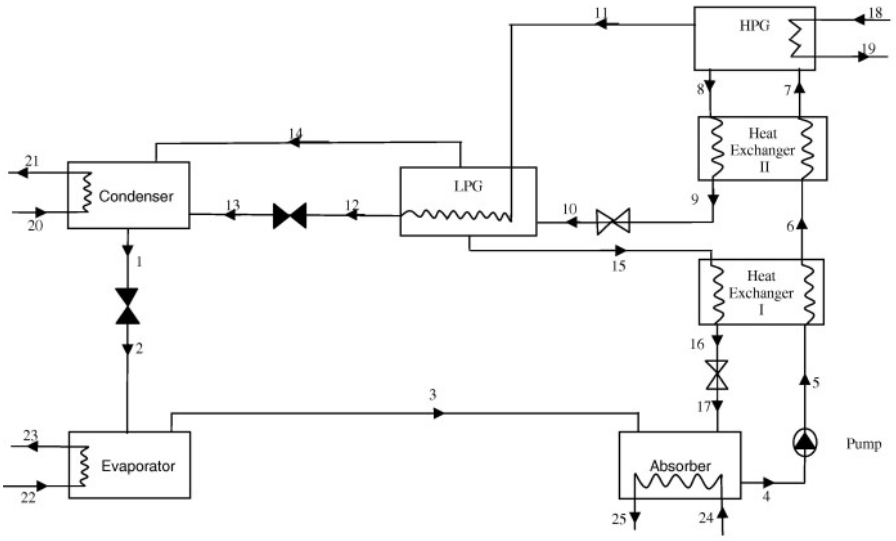

Figure 2.10: Schematic diagram of double-effect absorption cooling system.

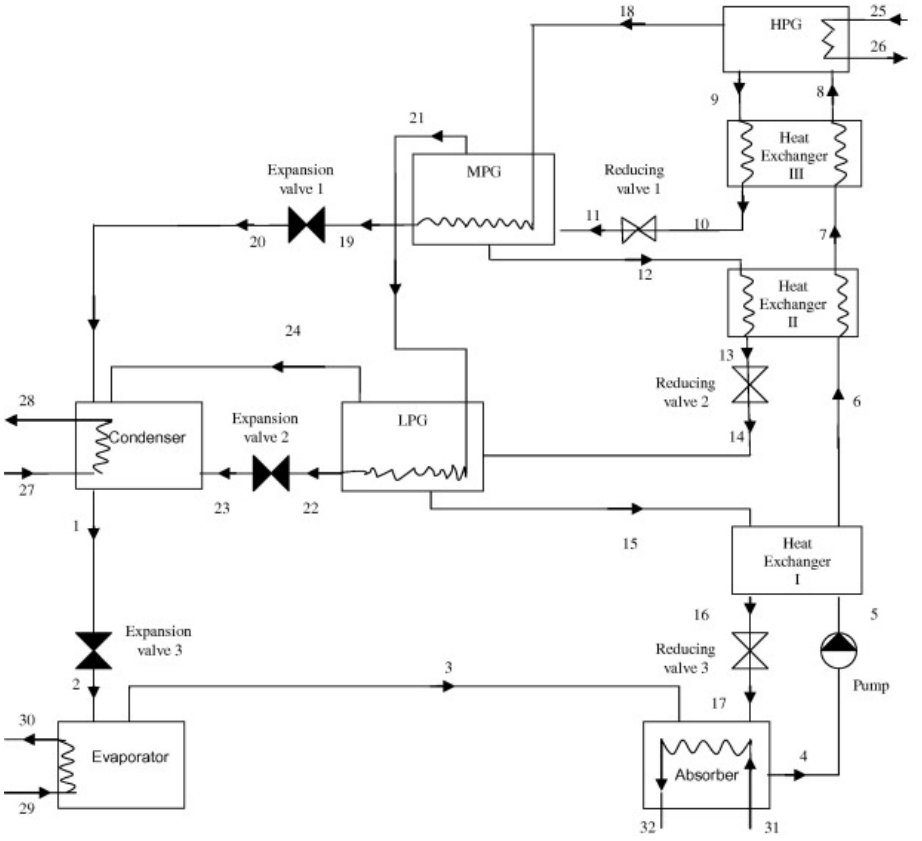

Figure 2.11: Schematic diagram of triple-effect absorption cooling system.

The effect of heat source temperature on cooling capacity and COP for different lithium bromide solution concentrations are shown in Figures 2.12 and 2.13, respectively. According to Figure 2.12, the effect of lithium bromide solution concentration on the cooling capacity is barely negligible, while its effect on the cooling performance is slightly considerable as shown in Figure 2.13. Reducing the lithium bromide solution concentration in the generator results in decrease of heat needed to generate water vapor, and this, in turn, results in higher COP. For optimum operation condition, it is suggested to operate with lithium bromide solution concentration in the range of 50-60%.

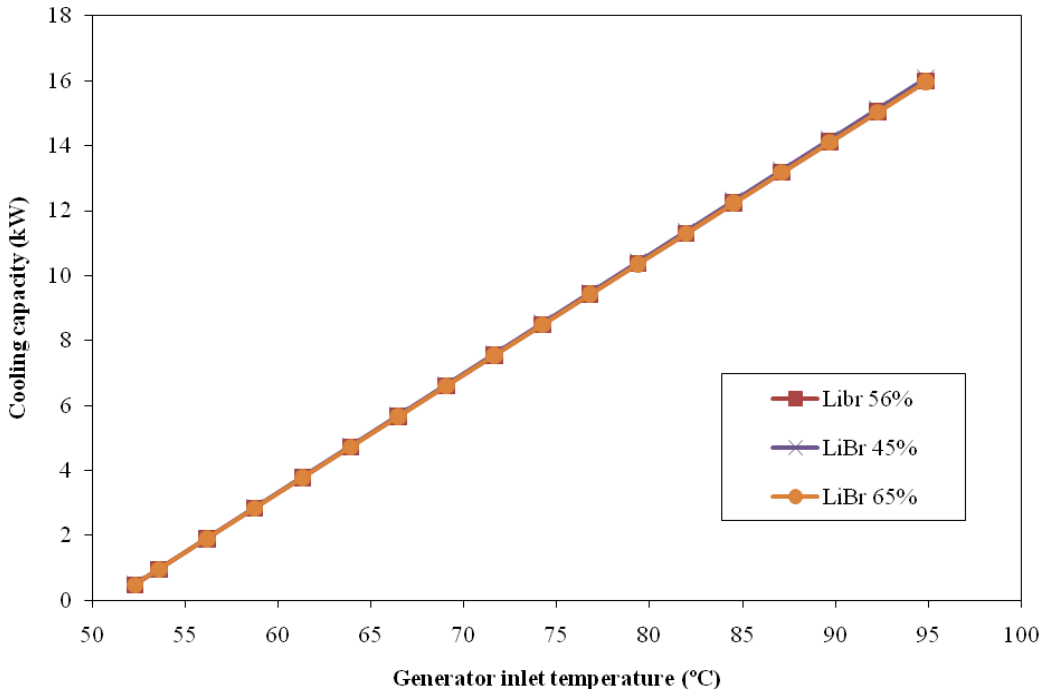

Figure 2.12: Effect of generator inlet temperature on cooling capacity for different LiBr solution concentrations.

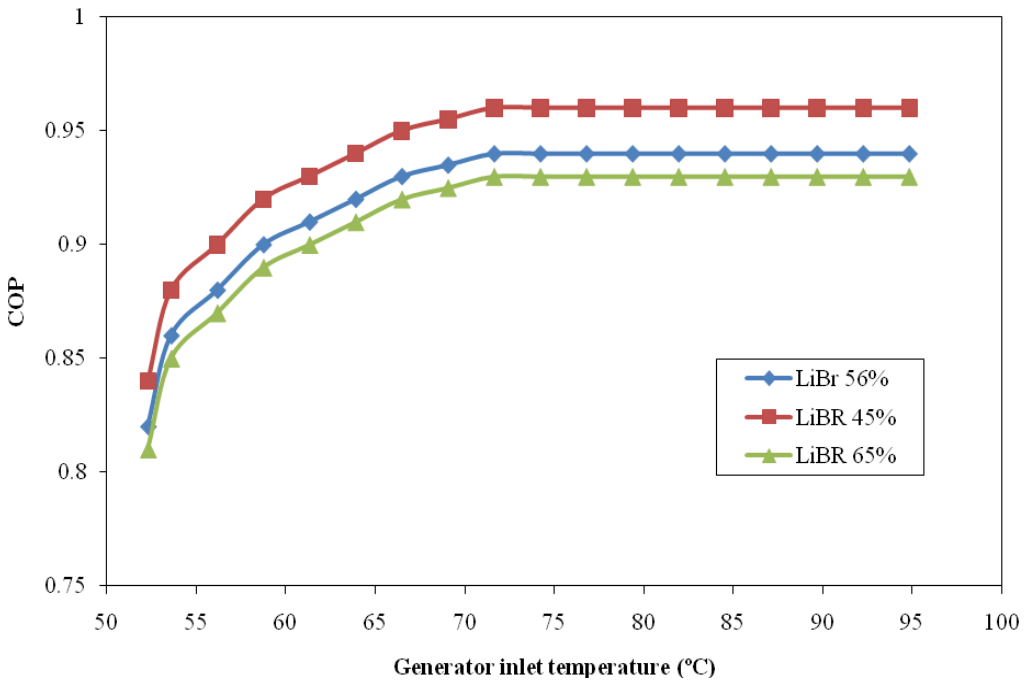

Figure 2.13: Effect of generator inlet temperature on COP for different LiBr solution concentrations.

Figures 2.14 and 2.15 show the effect of the inlet generator temperature on the cooling load and the cooling performance, respectively, for different P_{high} and P_{low} combinations. The first case is when condenser pressure is increased to P_{high} = 8 kPa and evaporator pressure is fixed at P_{low} = 0.9 kPa. In the second case, the condenser pressure is fixed at P_{high} = 6.601 kPa and the evaporator pressure is increased to P_{low} = 2.0 kPa. Both cases are compared with the normal condition of P_{high} = 6.601 kPa and P_{low} = 0.9 kPa. Increasing the condenser pressure (P_{high}) barely decreases the cooling load and so on the COP of the system decreases. In the other hand, increasing the evaporator pressure (P_{low}) barely increases the cooling load and so on the COP of the system increases. In the first case, when condenser pressure (P_{high}) is increased, the generator consumes more energy, and this causes the COP to decrease. While in the second case, where the

evaporator pressure (P_{low}) is increased, less energy is needed to generate water vapor, and thus the value of COP in this case is higher.

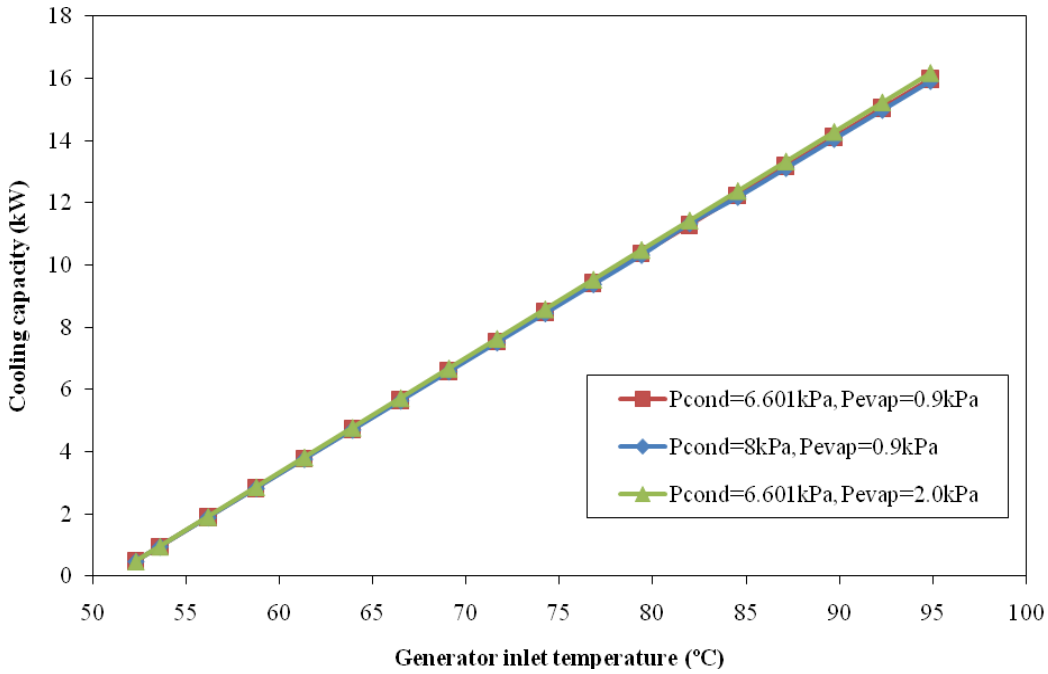

Figure 2.14: Effect of generator inlet temperature on cooling capacity for different P_{high} and P_{low} combinations.

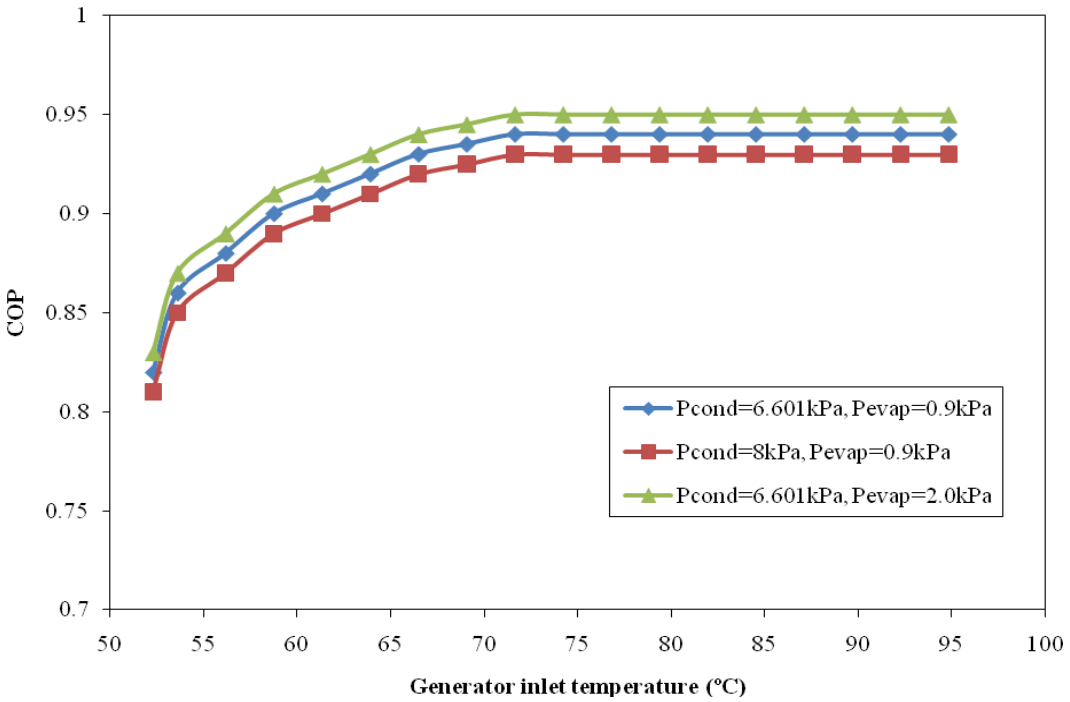

Figure 2.15: Effect of generator inlet temperature on COP for different P_{high} and P_{low} combinations.

The effect of varying the inlet generator temperature on the cooling load and cooling performance for different mass flow rates entering the generator is shown in Figure 2.16. The cooling capacity and cooling performance have the same behavior as previously explained. It is noticed that there are no improvements in the cooling capacity or the cooling performance when varying the inlet generator temperature for different mass flow rates. Once the mass flow rate increased, the simulation shows that the enthalpy is decreased and the amount of energy needed for the generator is maintained the same. This is true since the cooling performance maintains the same. On the other hand, increasing the mass flow rate causes more heat transfer in the solution heat exchanger, and so the surface area of the solution heat exchanger should be increased. In

the economic point of view, the mass flow rate should be optimized for smallest size of the solution heat exchanger.

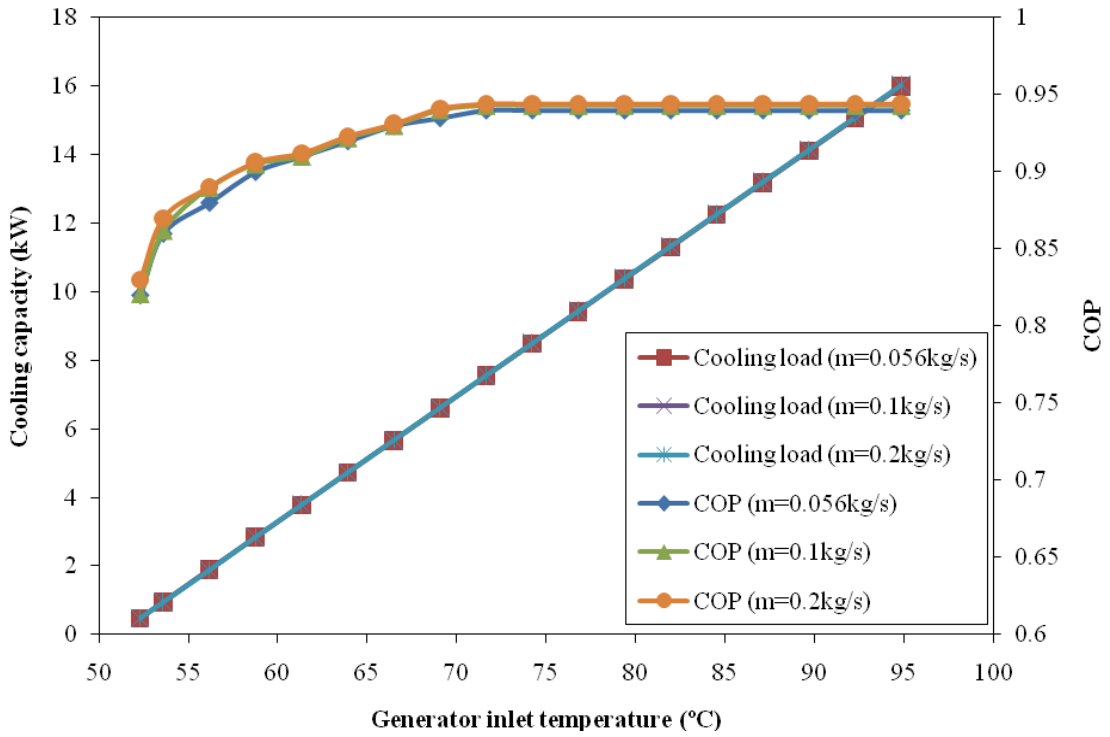

Figure 2.16: Effect of generator inlet temperature on cooling capacity and COP for different mass flow rates.

The model is used to find the cooling capacity and performance of the solar-powered absorption cooling system during a typical year in Tampa, Florida climate. Figure 2.17 shows the hourly variation for cooling capacity for Tampa, Florida weather condition during the months of January, April, August and November. The cooling capacity is gradually increasing during the morning hours starting around 7:00 am until it reach its maximum capacity around noon. Then, it decreases until sunset around 6:00 pm. In April, the cooling capacity reaches maximum due to the high solar isolation at this

time of the year. The cooling capacity simulated is also a function of solar intensity only. During the cold season, November and January, the cooling capacity is reduced.

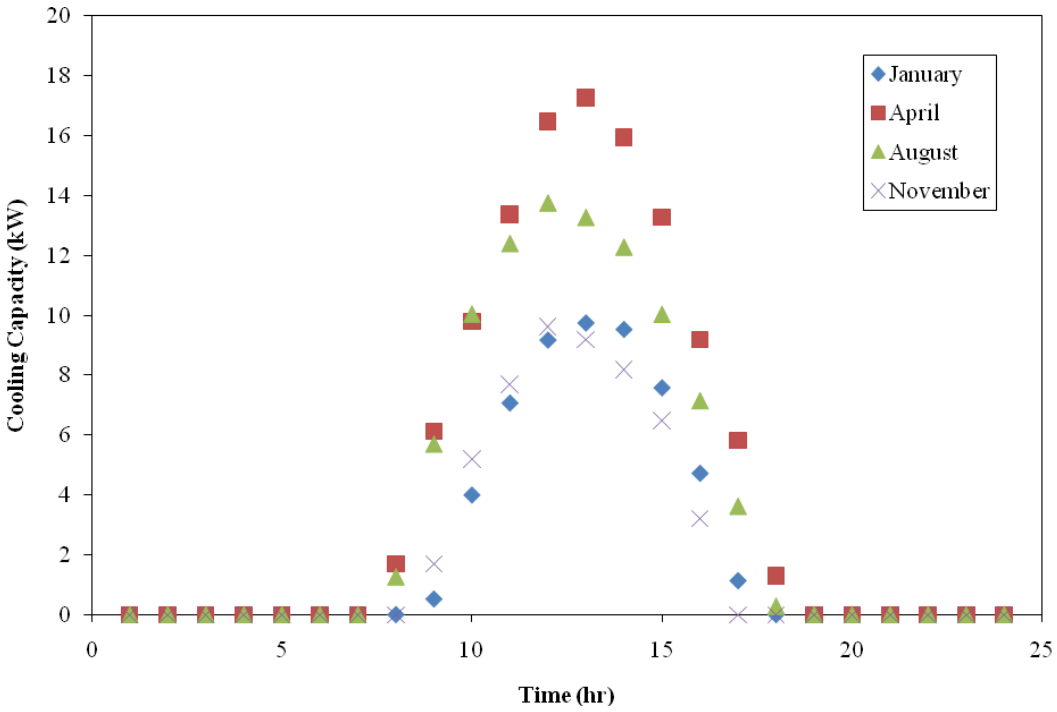

Figure 2.17: Model hourly cooling capacity for Tampa, Florida climate.

The coefficient of performance for the system model during a typical year in Tampa, Florida climate is shown in Figure 2.18. For the whole year, the system performance is stable during sunlight and the coefficient of performance is found to be around 0.94.

This system is suitable for hot weather such as Tampa's climate, despite the first cost for such systems, it could help to minimize the use of fossil fuel, reduce electricity demand and the use of CFCs.

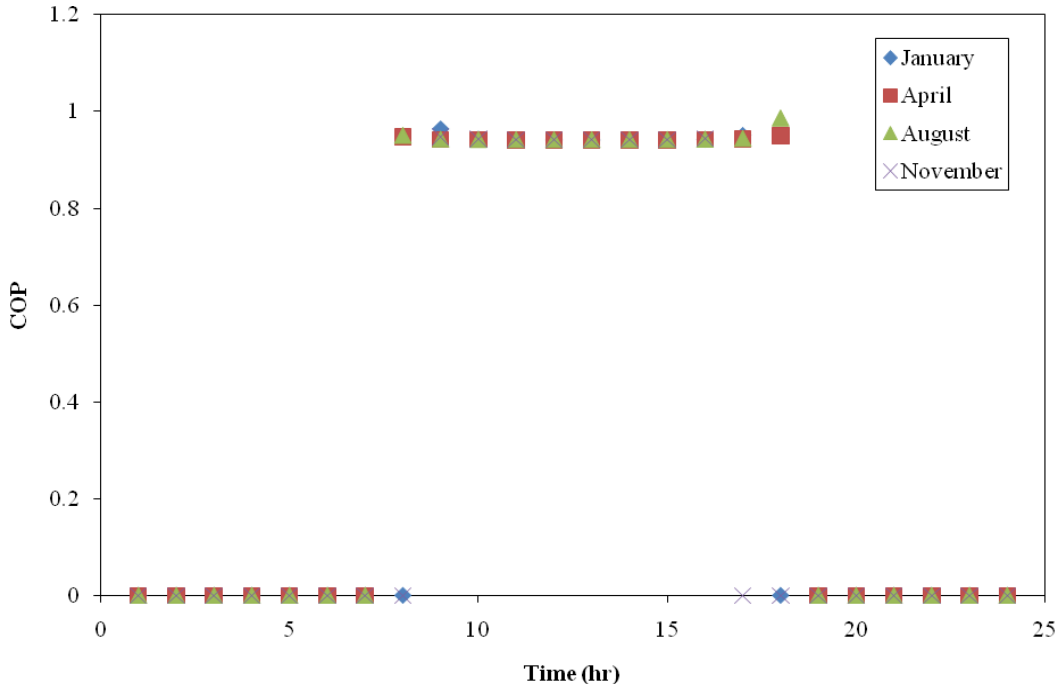

Figure 2.18: Model hourly coefficient of performance Tampa, Florida climate.

Chapter 3: Modeling of Supermarket Refrigeration/HVAC System for Simple Energy Prediction

3.1 Modeling and Simulation

A model was developed for a typical supermarket based on data prepared by the Food Marketing Institute Energy Committee and the information presented by references [39] and [40]. The layout for this typical supermarket is shown in Figure 3.1. The store description is as follows:

Store floor area:	3716 m^2 (40,000 ft^2)
Conditioned space:	2787 m^2 (30,000 ft^2)
Air supply rate:	14.16 m^3/s (30,000 cfm)
Outside ventilation air:	1.84 m^3/s (3900 cfm)
Hours of operation:	24 hours/day
People in store:	180 maximum. 92W/person (315 Btuh/person) sensible and 75W/person (255 Btuh/person) latent. People occupancy schedule is shown in Figure 3.2.
Indoor conditions:	24ºC (75ºF), variable relative humidity
Supply air conditions:	13ºC (55ºF), 95% relative humidity

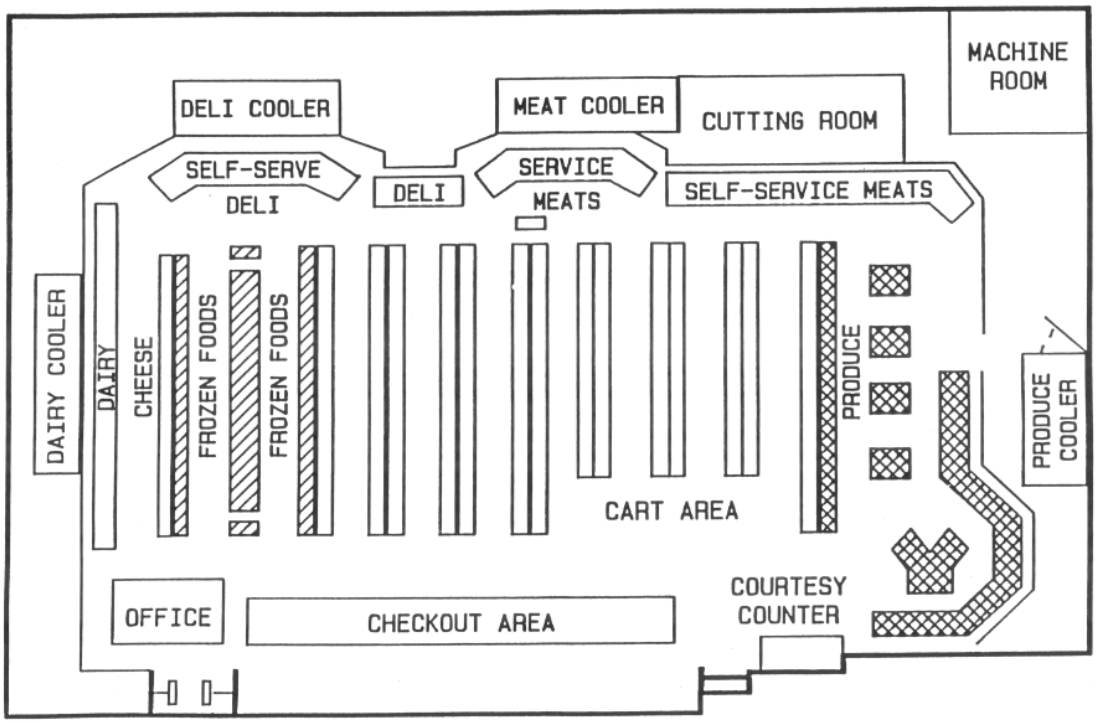

Figure 3.1: Layout of typical supermarket.

The installed refrigerated display cases capacity were set as follow: medium temperature horizontal single shelf display at [73m (240ft)], medium temperature vertical multi-shelf display at [73m (240ft)] and low temperature closed door within a reach-in of [91m (300ft)].

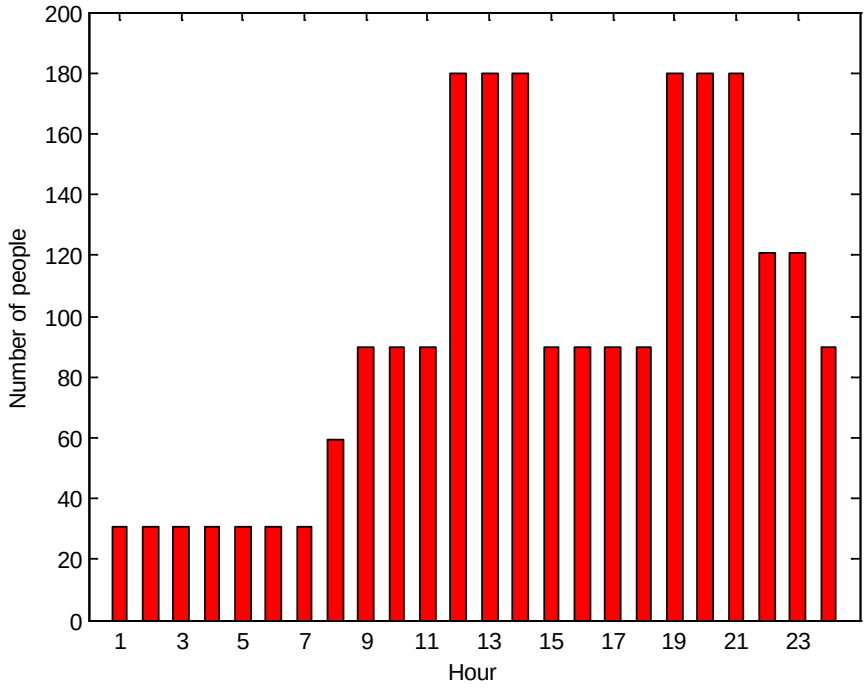

Figure 3.2: Schedule of people occupancy in supermarket model.

The hourly outdoor weather condition for Tampa, Florida is averaged for the years 2000-2010 [41] and illustrated in Figure 3.3. The hourly moisture balance was performed on the supermarket for a typical 24-hour day and averaged over the years 2000-2010. The annual effect can be obtained from the averaged weather data. The moisture balance, in terms of the latent energy balance is given by the following equation:

$$QL_{\text{space}} + QL_{\text{infil}} = QL_{\text{people}} + QL_{\text{produce}} + QL_{\text{meat}} + QL_{\text{bakery}} - QL_{\text{display case}} \quad (9)$$

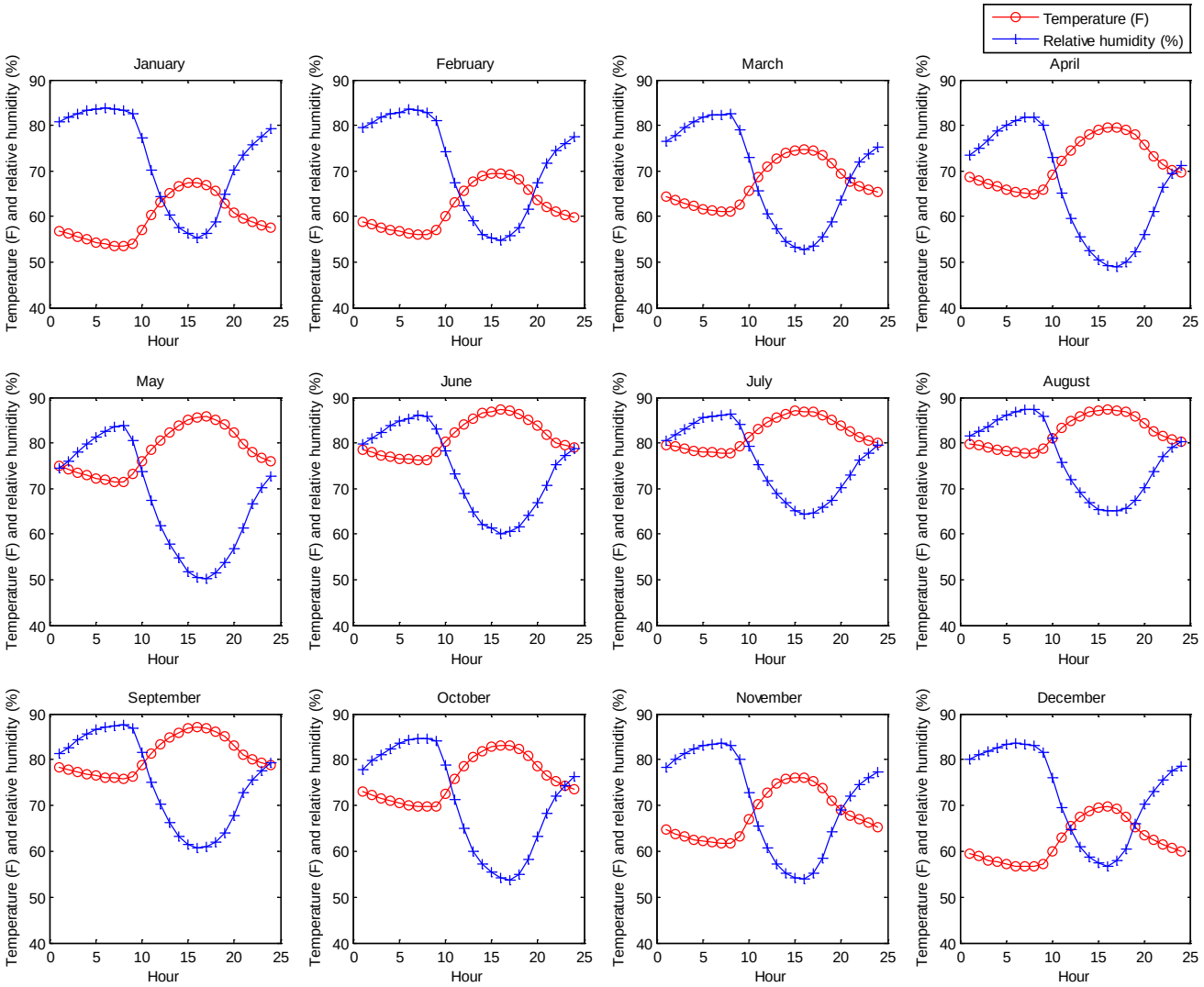

Figure 3.3: Annual average hourly outdoor temperature and relative humidity in variation Tampa, Florida (2000-2010).

The moisture balance states that the net moisture loss due to the building envelope and the operation of the air-conditioning equipment is balanced by the net production of moisture within the supermarket. The terms of the moisture equation are calculated from the following equations and thermal conditions:

$$QL_{\text{space}} = 3010\ q_{\text{space}}\ (w_{\text{space}} - w_{\text{supply}}) \tag{10}$$

$$QL_{\text{infil}} = 3010\ q_{\text{infil}}\ (w_{\text{space}} - w_{\text{outside}}) \tag{11}$$

$$QL_{\text{people}} = 0.075\ \text{NP} \tag{12}$$

$$QL_{\text{produce}} = 0.4103\ \text{kW} = 1400\ \text{Btu/hr}\ \text{(constant for 24 hours)} \tag{13}$$

$$QL_{\text{meat}} = 0.4103\ \text{kW} = 1400\ \text{Btu/hr}\ \text{(from 5am to 10am)} \tag{14}$$

$$QL_{\text{bakery}} = 3.517\ \text{kW} = 12000\ \text{Btu/hr}\ \text{(from 5am to 10pm)} \tag{15}$$

where,

$$q_{\text{infil}} = \left(44.5\text{NP} - 0.095\text{NP}^2 + 10^{-4}\text{NP}^3\right)\Delta P_{build}$$

$$q_{\text{space}} = 14.16\ \text{m}^3/\text{s} = 30{,}000\ \text{cfm}$$

$$\Delta P_{build} = 4.02\ \text{mm}\ \text{H}_2\text{O} = 0.16\ \text{in}\ \text{H}_2\text{O}$$

The major component of the display case model ($QL_{display\ case}$), is given by the air curtain. A strong heat and mass transfer exist within the air curtain as it separates the internal and external environment as shown in Figure 3.4. Figure 3.4 illustrates a vertical multi-shelf refrigerated display case, a typical horizontal single shelf refrigerated display case and standard closed door reach-in refrigerated case. The correlation of Ge and Tassou [26] was used for the air curtain of the refrigerated display cases. The four main parameters that affect the heat transfer of air curtain are the store air enthalpy, the dry-bulb temperature of the air curtain supply, display case air temperature or the air

temperature differential between the display case and the curtain supply, and air curtain properties such as: air curtain velocity and length. The air curtain thickness effect is included as part of the curtain velocity, which is generally presented by the mass flow rate. In the current work, the effect of air curtain length is ignored by the assumption of a unit length. In addition, Ge and Tassou [26] correlation was used to predict the heat transfer of horizontal and closed door reach-in refrigerated display cases and vertical multi-shelf refrigerated display cases. This is validated as part of the sensitivity analysis. The design specifications of Howell and Adams [13] for different display cases are shown in Table 3.1. In general, the following correlation was used to predict the heat transfer of air curtain for any display case:

$$Q_{\text{air curtain}} = [c_1 h_{\text{space}}^2 + c_2 h_{\text{space}} + c_3 (T_{\text{case}} + \Delta T)^2 + c_4 (T_{\text{case}} + \Delta T) + c_5 h_{\text{space}} (T_{\text{case}} + \Delta T) + c_6] \dot{m}_a \quad (16)$$

where,

$$h_{\text{space}} = 1.0 T_{\text{space}} + w_{\text{space}} (2501.3 + 1.86 T_{\text{space}}) \quad (17)$$

and c_1–c_6 are constants, which can be correlated from the simulation results of Ge and Tassou [26]. The correlated results of c_1–c_6 constants are shown in Table 3.2.

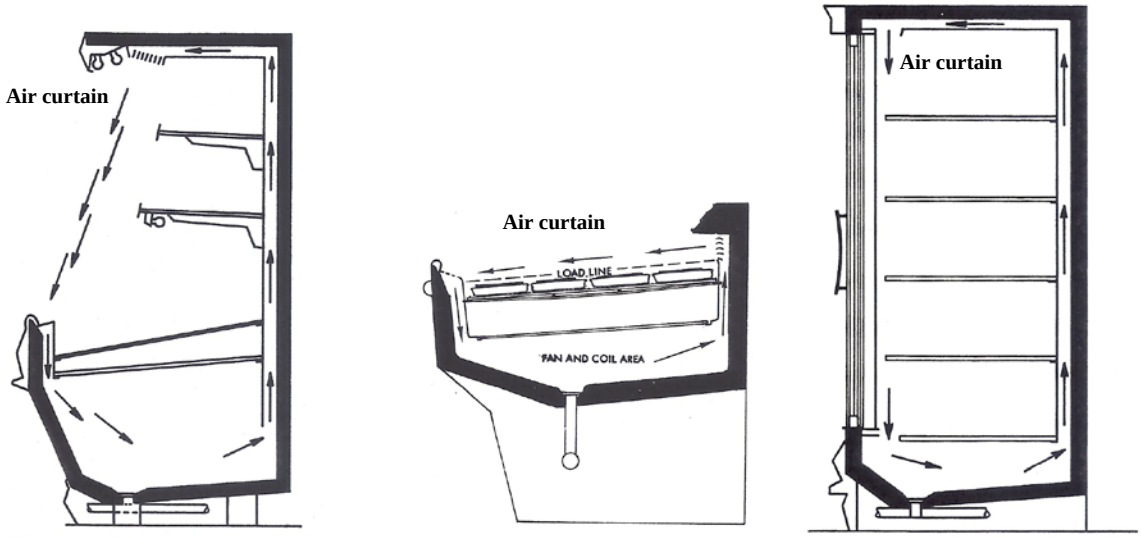

Figure 3.4: Typical refrigerated display cases: (a) Vertical multi shelf (b) Horizontal single shelf (c) Closed door reach-in [28].

Table 3.1: Design specifications for different types of refrigerated display case [13].

Case Type	Orientation	Case length m (ft)	Case Temp ºC (ºF)	Air curtain supply Temp ºC (ºF)	Air curtain velocity m/s (fpm)	Air curtain thickness m (in)
Medium Temp Single shelf	Horizontal	73 (240)	4.4 (24)	2 (35)	0.56 (110)	0.102 (4.0)
Medium Temp Multi-shelf	Vertical	73 (240)	3 (37)	0 (32)	1.32 (260)	0.114 (4.5)
Low Temp Reach-in	Vertical	91 (300)	-2 (29)	-4.4 (24)	0.68 (133)	0.076 (3.0)

Table 3.2: The correlated constants c_1-c_6 [26].

c_1	c_2	c_3	c_4	c_5	c_6
-0.180	303.180	-0.781	216.309	-0.448	509.975

ASHRAE [42] gave the percentage of latent load for each type of refrigerated display case; 12% for single shelf, 19% for multi-shelf and reach-ins respectively. These values take in account the performance of display cases with a store relative humidity

maintained of 55%. The latent load percentage values for each type of refrigerated display case decreases at lower relative humidity and affects the simulated store relative humidity. However, the latent load percentage values for each type of refrigerated display case are taken as the maximum to prevent any frost formation and maintain the desired temperature of products. In this work, MATLAB [43] software was used to simulate the latent heat balance inside the supermarket. Steady state simulations were carried out on an hourly basis for the typical day in each month using the averaged annual data obtained from [41] using the weather conditions of Tampa, Florida during the period of 2000-2010. The average of these data are illustrated in Figure 3.3. The store temperature is maintained at 24ºC (75ºF). The hourly moisture balance, equation (9), was used along with the air curtain heat equation, equation (16), and resulted in a relative humidity profile for the typical day inside of the store. Figure 3.5 shows a flow-diagram of how the simulation works using input data. The output includes an hourly store relative humidity for a typical day of each month of the year.

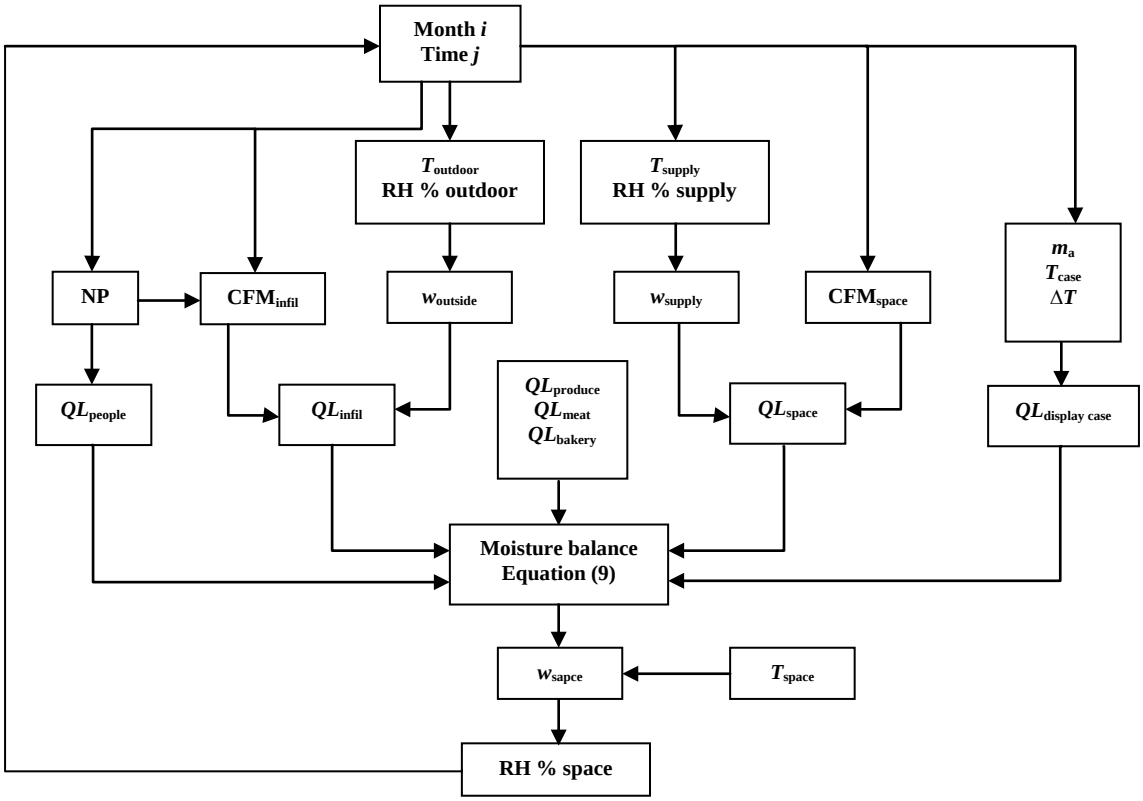

Figure 3.5: Information-flow diagram for store relative humidity simulation.

3.2 Simulation Results

The results from the supermarket model simulations were run for the typical 24-hour day for a year. The results present the store relative humidity each hour for typical day each month. Figure 3.6 illustrates an hourly plot of store relative humidity for typical year in Tampa, Florida. The store relative humidity remains in the range of 40-60% from January till May and from October till December. During the summer season from June till September, the store relative humidity increases above 60% during noon times. This is obvious because of the hot and humid weather in Tampa, Florida during noon times.

The hourly values for the all months simulated have been averaged separately and are presented in Table 3.3. The monthly store relative humidity in Table 3.3 remains in the range of 40-60%. These results are dependent on the assumptions made for the supermarket model. However, these results appear to be typical for a supermarket with air-conditioning located in a weather condition similar to Tampa, Florida. The variation expected in the store relative humidity would be in the range of 40-60% for hot and humid climates. The results in Table 3.3 should be considered of what is anticipated in a supermarket rather than using a design store relative humidity of 55%. Thus, changes in the refrigerated display case energy can be estimated for increases or decreases in store relative humidity, and that resulted in changes in the operation of the supermarket air-conditioning system. This will be analyzed later on in the energy consumption changes section.

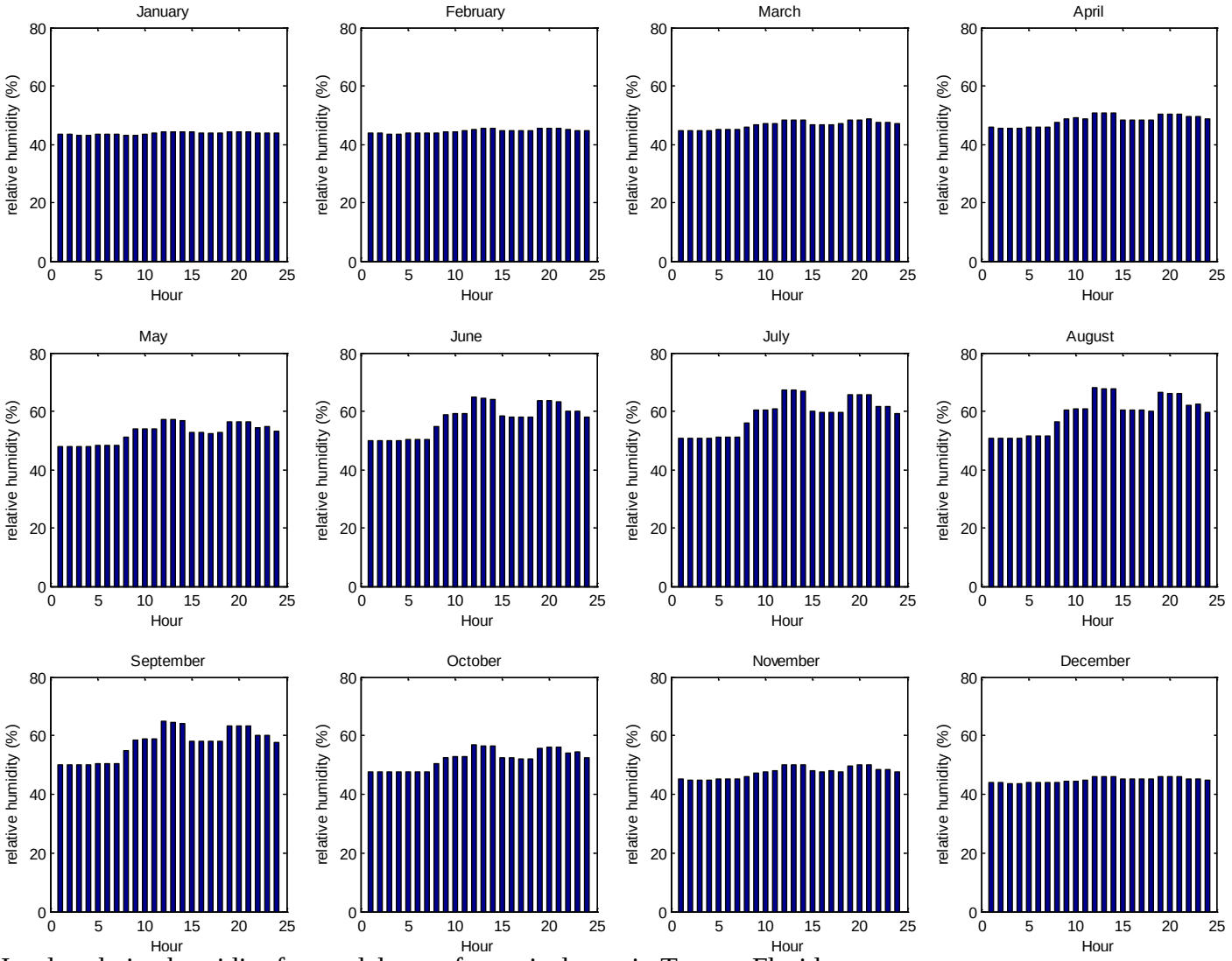

Figure 3.6: Hourly relative humidity for model store for typical year in Tampa, Florida.

Table 3.3: Average store relative humidity for supermarket model simulated at 24ºC (75ºF) for each month for Tampa, Florida.

Month	Average relative humidity inside store (%)
January	43.72
February	44.51
March	46.66
April	48.24
May	52.57
June	57.40
July	58.87
August	59.28
September	57.41
October	52.08
November	47.48
December	44.92

3.3 Sensitivity Analysis

The performance of the model representing the supermarket refrigeration system needs to be evaluated for different outdoor conditions each month for the whole year. The incorporation of air curtain correlation for latent heat calculation of the refrigerated display cases has been evaluated by a comparison with pervious simulation model [39] and existing experimental data [18] for the weather conditions of Tampa, Florida. The supermarket model developed by [39] has the same description of the current model, however, the current model includes the effect of store relative humidity on refrigerated display cases assigned in the moisture balance. Also, it can simulate the store relative humidity on an hourly basis. Figures 3.7 and 3.8 show comparison of the hourly store relative humidity of [39] and the current model for the months of January and August, respectively. In January, the relative humidity inside the store exhibits stable behavior for the current model. This is because the current model has a precise representation of the display cases, and they are affected by the store relative humidity. The results of the current model are comparable with model [39]. The discrepancy is because the input weather data used for the model in [39] is interpolated and extrapolated, while it is taken hour by hour in the current model. In the month of August, Figure 3.8, there is an increase in the store relative humidity around noon. This is due to the high temperature and high relative humidity of the weather during summer season. However, the results of the current model are comparable with model [39].

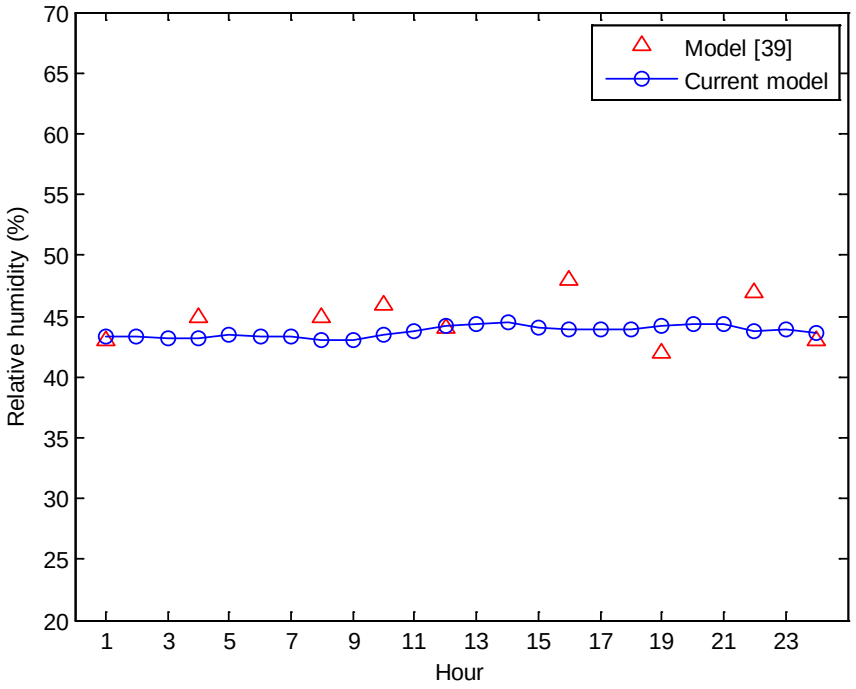

Figure 3.7: Comparison of hourly relative humidity for [39] and supermarket model for month of January.

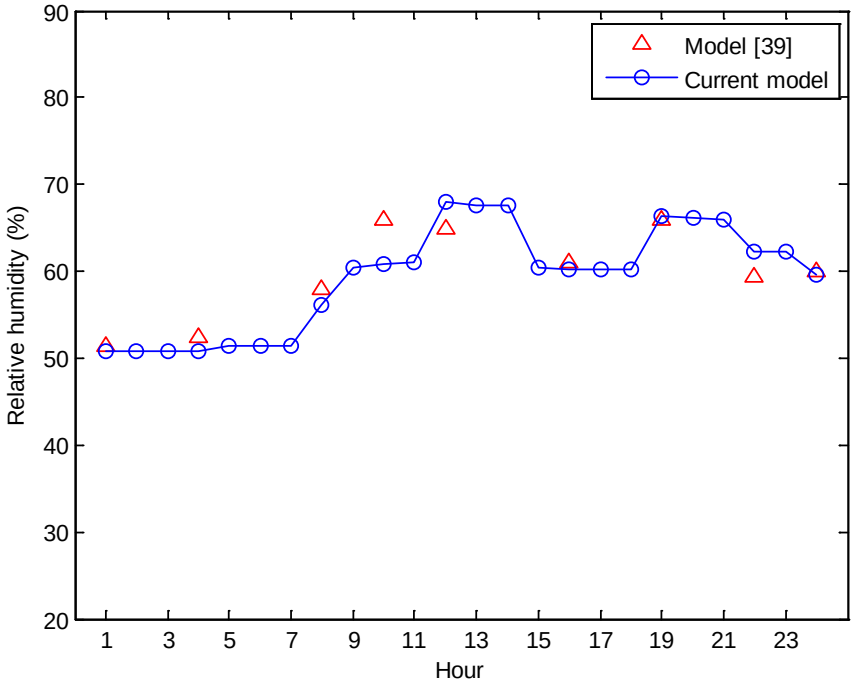

Figure 3.8: Comparison of hourly relative humidity for [39] and supermarket model for month of August.

For more precise comparison, the average monthly relative humidity inside the store for [39] and the current model are calculated and shown in Figure 3.9. The current model shows matching trend with [39] where maximum store relative humidity of approximately 60% in August and minimum store relative humidity of approximately 45% in January.

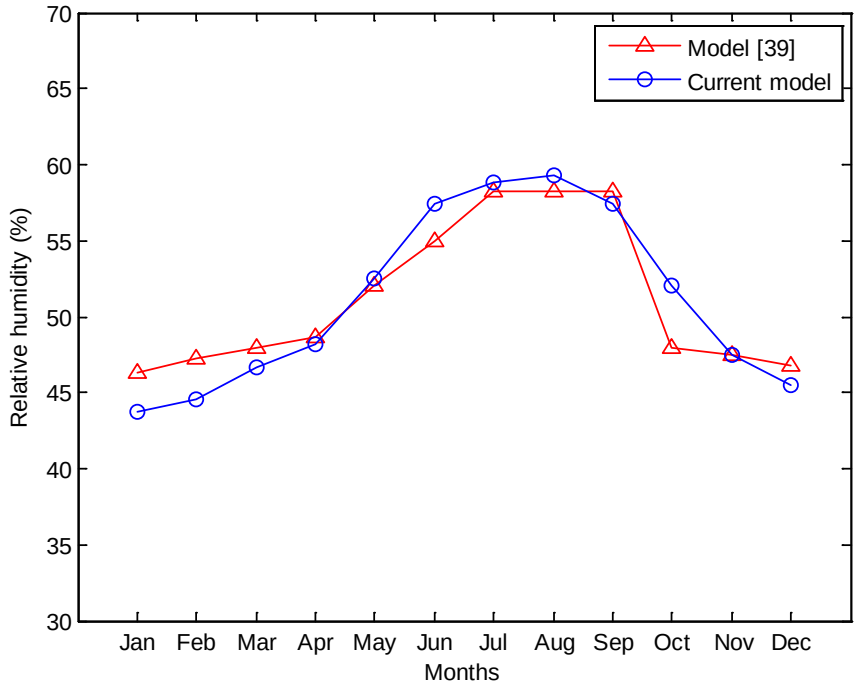

Figure 3.9: Comparison of average monthly relative humidity for [39] and supermarket model for Tampa, Florida.

Comparison of the current model with available experimental data of [22] is shown in Figure 3.10. For the same design condition in supermarket in Auckland, New Zealand, the current model simulates the store relative humidity for a typical day in December 2004. It is shown that the results are comparable with experimental data.

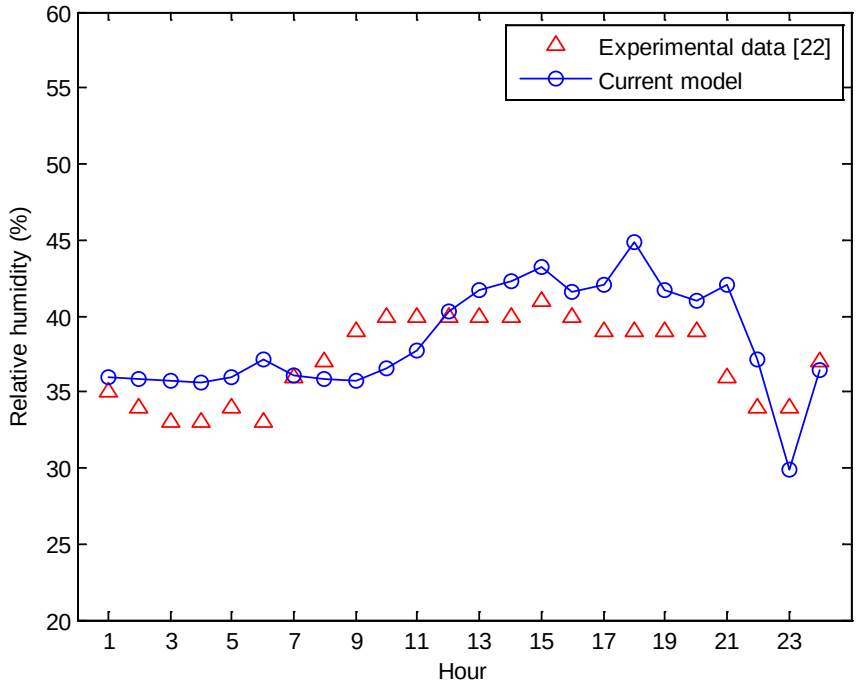

Figure 3.10: Comparison of relative humidity for experimental data [22] and supermarket model for a typical day in Auckland, New Zealand in December 2004.

Figure 3.11 shows a comparison of the current model with the experimental data of [18]. Figure 10 shows the maximum, minimum and averaged store relative humidity for a typical store located in Tampa, Florida. There is an increase in the store relative humidity during the summer season beginning in May and ending in September. The current model has a trend in the range of experimental data. Also, the percentage values assumed for latent heat calculation for the refrigerated display cases are maximum, so for more precise results, they need to be varied with store relative humidity. Overall, the representation of display cases brought by the air curtain energy equation (16) is feasible to be used in the supermarket model for latent heat calculations.

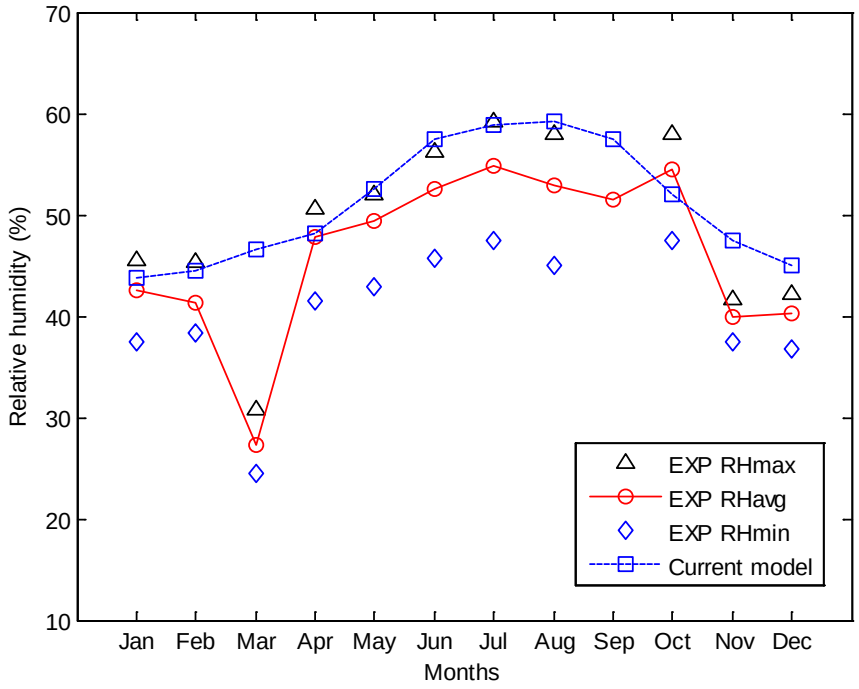

Figure 3.11: Comparison of relative humidity for experimental data [18] and supermarket model.

3.4 Energy Consumption Analysis

The modern supermarket is the greatest consumer for refrigeration energy within the commercial sector. In the United States, the electrical consumption in supermarkets presents 2.3% of the national electric use, and 50% of the total retail store energy is consumed by the refrigerated display cases and air-conditioning systems [42]. The relationship between the store HVAC and the refrigeration is very important in terms of the overall energy consumption of the supermarket. Howell [13-15] developed several procedures to calculate the savings in store energy requirement by the knowledge of the indoor store relative humidity distribution during the year. He showed the influence of the indoor relative humidity on the refrigerated display case energy consumption. The method developed will be used in this work to evaluate the effect of store relative humidity on display case energy requirements. These energy requirements were divided into three components: energy required by the case refrigeration, energy required by anti-sweat heaters, and energy required for defrost. The store relative humidity affects all three of these components. Each of these refrigerated display case loads were evaluated on a percent change basis, compared to operation at relative humidity of 55%, and are given by the following equations [13]:

$$TP = QRH / QR \tag{18}$$

$$DP = DFRH / DF \tag{19}$$

$$AP = ASWRH / ASW \tag{20}$$

where,

TP: ratio of display case refrigeration energy requirement when operated at a relative humidity other that 55%.

QRH: display case refrigeration energy requirement at a given relative humidity.

QR: display case refrigeration energy requirement at the design value of relative humidity of 55%.

DP: ratio of display case defrost energy requirements when operated at a relative humidity other than 55%.

DFRH: defrost energy requirement for the display case at a given relative humidity.

DF: defrost energy requirement for the display case at the design value of relative humidity of 55%.

AP: ratio of display case anti-sweat heater load when operated at a relative humidity other than 55%.

ASWRH: anti-sweat heater energy requirement for the display case at a given relative humidity.

ASW: anti-sweat heater energy requirement for the display case at the design value of relative humidity of 55%.

Howell [14] evaluated the values for TP and DP when the store temperature was kept at 24ºC (75ºF). These values are listed in Tables 3.4 and 3.5, and can be used for a wide variation in types of display cases as well as a full variation of case sizes and operating conditions. TP and DP values for multi-shelf refrigerated vertical display cases are listed in Table 3.4, while Table 3.5 lists the values for single-shelf horizontal display cases. Values for AP are evaluated also for different display case temperatures as shown in Table 3.6.

Table 3.4: Load change factors for refrigeration energy (TP) and case defrost energy (DP) at various relative humidities and 24ºC (75ºF) ambient for multi-shelf vertical display cases [13].

RH	DP	TP	DP	TP
	Multi-shelf meat		Multi-shelf dairy	
30	0.417	0.733	0.259	0.647
35	0.532	0.786	0.406	0.717
40	0.648	0.839	0.553	0.788
45	0.766	0.893	0.703	0.858
50	0.882	0.947	0.851	0.929
55	1.000	1.000	1.000	1.000
60	1.118	1.054	1.149	1.071
65	1.235	1.108	1.299	1.142
	Multi-shelf deli		Closed door ice cream	
30	0.321	0.683	0.527	0.825
35	0.455	0.746	0.620	0.859
40	0.590	0.809	0.715	0.895
45	0.727	0.873	0.812	0.929
50	0.862	0.936	0.905	0.964
55	1.000	1.000	1.000	1.000
60	1.137	1.063	1.095	1.035
65	1.273	1.127	1.191	1.070
	Closed door frozen food		Multi-shelf frozen food	
30	0.519	0.814	0.534	0.829
35	0.614	0.851	0.626	0.862
40	0.710	0.888	0.719	0.897
45	0.807	0.925	0.813	0.931
50	0.903	0.962	0.906	0.965
55	1.000	1.000	1.000	1.000
60	1.096	1.037	1.094	1.035
65	1.193	1.074	1.188	1.069
	Multi-shelf produce			
30	0.290	0.646		
35	0.430	0.715		
40	0.571	0.785		
45	0.715	0.856		
50	0.856	0.927		
55	1.000	1.000		
60	1.143	1.070		
65	1.286	1.141		

Table 3.5: Load change factors for refrigeration energy (TP) and case defrost energy (DP) at various relative humidities and 24ºC (75ºF) ambient for single shelf horizontal display cases [13].

RH	DP	TP	DP	TP
	Single-shelf meat		Single-shelf frozen	
31	0.465	0.799	0.553	0.853
34	0.536	0.826	0.612	0.872
38	0.609	0.853	0.673	0.892
41	0.684	0.881	0.736	0.912
44	0.760	0.910	0.799	0.933
48	0.838	0.939	0.865	0.955
51	0.918	0.968	0.931	0.978
55	1.000	1.000	1.000	1.000
58	1.083	1.031	1.069	1.021
62	1.169	1.064	1.141	1.044
	Single-shelf ice cream		Single-shelf produce	
31	0.558	0.865	0.363	0.774
34	0.617	0.881	0.448	0.803
38	0.678	0.900	0.535	0.834
41	0.739	0.919	0.624	0.866
44	0.802	0.939	0.715	0.897
48	0.867	0.958	0.807	0.929
51	0.932	0.979	0.902	0.965
55	1.000	1.000	1.000	1.000
58	1.068	1.022	1.099	1.035
62	1.139	1.044	1.201	1.070

Table 3.6: Load change factor (AP) for anti-sweat energy requirements for all types of display cases at 24ºC (75ºF) ambient [13].

	Display case temperature			
Store RH (%)	5ºC (41ºF)	3ºC (37ºF)	-2ºC (29ºF)	-22ºC (-7ºF)
65	1.28	1.23	1.16	1.07
60	1.15	1.12	1.09	1.04
55	1.00	1.00	1.00	1.00
50	0.84	0.87	0.91	0.96
45	0.67	0.73	0.81	0.91
40	0.48	0.58	0.70	0.86
35	0.27	0.41	0.57	0.81

In order to calculate the savings in energy in the operation of the display cases, it is necessary to establish its standard energy consumption for the refrigeration energy, defrost energy and anti-sweat heater energy. The defrost energy and anti-sweat heaters energy are estimated by Howell and Adams [13] and given in Table 3.7. Equation (16) is used to calculate the refrigeration energy for the display cases at 24ºC store temperature and relative humidity of 55%. The medium temperature single shelf horizontal units of length 240 ft (73m) has calculated refrigeration energy of 628 Btu/hr-ft and assumed to have an energy efficiency ratio (EER) of 8 Btu/Wh. The medium temperature multi-shelf vertical units of length 240 ft (73m) has calculated refrigeration energy of 1735 Btu/hr-ft and assumed to have an energy efficiency ratio (EER) of 7 Btu/Wh. The low temperature closed door reach-in units of length 300 ft (91m) has calculated refrigeration energy of 536 Btu/hr-ft and assumed to have an energy efficiency ratio (EER) of 6 Btu/Wh. Thus, kW demand and the kWh per month can be calculated as shown in Table 3.7 for the three display cases. Howell and Adams [13] gave approximate values for defrosts energy and anti-sweat heaters energy as shown in Table 3.7. They are taken at the rated store relative humidity of 55%. The number of defrosts varied from 2 to 4 per day and consumed 16,667 kWh per month and the total anti-sweat heater load was 23.4 kW which consumed 16,850 kWh per month. The annual energy load for the refrigeration, defrost and anti-sweat heaters is about 1,311,000 kWh. Normally, this load is about 70% of the supermarket's total annual energy consumption.

Table 3.7: Display case refrigeration energy for simulated store at 24ºC (75ºF) and 55% relative humidity.

Case Type	Orientation	Case length m (ft)	Case Temp ºC (ºF)	Btu/ hr-ft	kW (Btu/hr)	EER	kW demand	kWh/ month
Medium Temp Single shelf	Horizontal	73 (240)	4.4 (24)	628	44 (150,906)	8	18.86	13,580
Medium Temp Multi-shelf	Vertical	73 (240)	3 (37)	1735	122 (416,600)	7	59.50	42,840
Low Temp Reach-in	Vertical	91 (300)	-2 (29)	536	47 (160,738)	6	26.79	19,289
Total		237 (780)	--	--	--	--	105.15	75,709
Defrost	2 to 4 per day							16,667
Anti-sweat heaters	23.4 kW							16,850

In order to evaluate savings in display case energy with reductions in ambient store relative humidity it is necessary to determine TP, DP and AP at different store relative humidities. These three factors or modifiers can then be used with the energy loads given in Table 3.7 to estimate energy requirements at the different store relative humidity. The average monthly relative humidity for supermarket model is determined and listed in Table 3.3. Assuming each month has the same number of days, the twelve months are averaged and resulting in an annual average store relative humidity of 51.1%. This seems to be a feasible value for the Tampa, Florida weather climate. Since display cases are designed for 55% ambient relative humidity, the actual annual energy requirement for the display cases for this supermarket model would be less than 1.31 million kWh as previously calculated.

To calculate the energy savings for these display cases, the three energy factors or modifiers are determined for the new store relative humidity of 51.1%. This is done using the information in Tables 3.4, 3.5 and 3.6. Values for TP, DP and AP are found for average annual store relative humidities of 51.1%, 45%, 40%, and 35% and listed in Table 3.8 for the three display cases. The values for TP, DP and AP are 1.0 for 55% RH. This is the reference point for upcoming results. Using the display case energy requirements at 55% relative humidity in Table 3.7, and energy modifiers listed in Table 3.8, annual energy requirements at various store relative humidities are estimated in Table 3.9. The total display cases energy load is separated into refrigeration energy, defrost energy and anti-sweat energy so that it can be compared with the actual situations. Notice from Table 3.8 that reducing the store relative humidity results in reduction in the total display cases energy requirements as mentioned previously.

Table 3.8: Display case energy modifiers for various average annual store relative humidities.

Average annual store relative humidity	51.1% RH			45% RH		
	TP	DP	AP	TP	DP	AP
Medium Temp Single shelf	0.966	0.904	0.882	0.905	0.738	0.688
Medium Temp Multi-shelf	0.945	0.884	0.899	0.858	0.703	0.730
Low Temp Reach-in	0.959	0.908	0.930	0.893	0.766	0.810
Average annual store relative humidity	40% RH			35% RH		
	TP	DP	AP	TP	DP	AP
Medium Temp Single shelf	0.855	0.594	0.510	0.811	0.470	0.312
Medium Temp Multi-shelf	0.788	0.553	0.580	0.717	0.406	0.410
Low Temp Reach-in	0.839	0.648	0.700	0.786	0.532	0.570

Table 3.9: Display cases annual energy requirements at various store relative humidities.

	55% RH	51.1% RH	45% RH	40% RH	35% RH
Refrigeration, kWh	908,508	864,908	795,260	738,682	682,649
Defrost, kWh	200,004	179,750	147,136	119,691	93,852
Anti sweat, kWh	202,200	182,696	150,167	120,646	87,081
Total, kWh	1,310,712	1,227,354	1,092,564	979,019	863,582

The percent savings in energy for the various components as well as the total display case energy savings for the various store relative humidities are given in Table 3.10. The base case for comparison is at store relative humidity of 51.1%. It may be noticed from Table 3.10 that for range of store relative humidity of 35-55%, the changes in energy requirements are approximately linear. These results show that for a 5% reduction in store relative humidity; the refrigeration load is reduced by 6.5%, the defrost load is reduced 15%, the anti-sweat heater load is reduced 16%, and the total display case load is reduced 9.25%.

Table 3.10: Percentage changes in energy for various store relative humidities (percent change compared to base case at 51.1% RH).

	55% RH	51.1% RH	45% RH	40% RH	35% RH
Total, kWh	1,310,712	1,227,354	1,092,564	979,019	863,582
Change %	+6.36	0.00	-10.98	-20.23	-29.64
Defrost, kWh	200,004	179,750	147,136	119,691	93,852
Change %	+10.13	0.00	-18.14	-33.41	-47.79
Anti-sweat, kWh	202,200	182,696	150,167	120,646	87,081
Change %	+9.65	0.00	-17.80	-33.96	-52.34
Refrigeration, kWh	908,508	864,908	795,260	738,682	682,649
Change %	+4.80	0.00	-8.05	-14.59	-21.07

In order to justify the reduction in store relative humidity, the percent increase in air-conditioning energy required to reduce the store relative humidity by 5% should be determined. Howell [15] estimated the annual air-conditioning energy requirement needed to maintain the store at 24ºC (75ºF) and relative humidity of 55%. They simulated a retail store, and found that for AC unit with energy efficiency ratio of 9.5 Btu/W-hr, and 2.812 watts cooling/watts power, the annual energy was estimated to be 478,600 kWh. When reducing the store relative humidity to 45%, the same AC unit would require 499,600 kWh, and for store relative humidity of 35%, 516,600 kWh was required. For our designed store relative humidity of 51.1%, the AC energy required is 486,790 kWh. Howell [15] also showed, in order to evaluate reasonable percent changes in energy for the total supermarket, lights and appliances annual energy are required and estimated as 300,000 kWh. These data are shown in Table 3.11 to compare changes in energy requirements at different relative humidities for each component of the store electric bill. From Table 3.11, it can be determined that for a 5% reduction in store relative humidity, there is about 4.82% reduction in the total store annual energy. Also, it can be determined that for each 1% reduction in store relative humidity, there is an approximate savings in annual store energy of 19,000 to 20,000 kWh.

Table 3.11: Changes in total store energy requirements at various relative humidities.

	55% RH	51.1% RH	45% RH	40% RH
Total display case annual energy, kWh	1,310,712	1,227,354	1,092,564	979,019
AC annual energy, kWh	478,600	486,790	499,600	508,100
Lights and appliances, annual energy, kWh	300,000	300,000	300,000	300,000
Total store annual energy, kWh	2,089,312	2,014,144	1,892,164	1,787,119
Saving realized by changing from 55% RH, kWh	--	75,168	197,148	302,193
Saving in kWh for each 1% reduction in RH, kWh	--	19,274	19,715	20,146
Percentage savings in total store energy by changing from 55% RH, %	--	3.60	9.44	14.46
Percent savings in total store energy for each 1% change in RH, %	--	0.92	0.94	0.96

Howell et al. [39] estimated the annual air-conditioning energy requirement needed to maintain the store at 24ºC (75ºF) and relative humidity of 51.2%. They found for a 5% reduction in store relative humidity, the display case refrigeration load reduced by 10%, and that results in total store energy load reduction of 4.7%. Because of the integration of store relative humidity within the air curtain correlation in the moisture balance, the current model shows a reduction in the display case refrigeration load by 9.25% for a 5% reduction in store relative humidity, while Howell et al. [39] model had a reduction in refrigeration load of 10%. However, the recommended relative humidity by Howell et al. [39], and the one determined in this work are comparable. Estimated store relative humidities by Howell et al. [39] and in the current model are 51.2% and 51.1%, respectively. The current model shows a reduction in the total store energy load by 4.84%, while Howell et al. [39], the load was reduced by 4.7%. This explains the sensitivity of the current model. In addition, the current model incorporate the effect of

store relative humidity with the refrigerated display cases assigned in the supermarket model.

The results of the sensitivity analysis and energy analysis show that the use of air curtain correlation is feasible to study the effect of relative humidity inside the retail store. This has been evaluated to be used for different types of display cases such as horizontal and closed door reach-ins type, and shows good agreement with previous models and experimental data. Thus, it can be employed for quick design calculation and for the simulation of different types of display cases within a supermarket model.

Chapter 4: Conclusions

4.1 Solar-Powered Single-Effect Absorption Cooling System

The greatest advantage of solar-powered absorption cooling system when compared to other cooling applications is the greater the sun radiation, the greater cooling performance that can be achieved by the solar refrigeration system. CHEMCAD model shows good trend for cooling capacity and COP when compared with previous models. In order to achieve higher COP, LiBr-H_2O mixture is good solution to be used in solar-powered absorption cooling system. According to the results, the cooling performance can be varied with LiBr solution concentration. The results show for higher cooling performance, optimized LiBr solution concentration is suggested. The effects of evaporator and condenser pressures and varying the mass flow rate on the cooling capacity and cooling performance are generally negligible as the results show. The cooling performance is assessed for typical year in Tampa, Florida weather condition, and the results show constant coefficient of performance of 0.94. Finally by considering the problem of pollution on the planet due to the burning of fossil fuels the adoption of solar energy to power absorption chillers, even with marginal economic benefits, should not be underestimated.

4.2 Modeling of Supermarket Refrigeration/HVAC System for Simple Energy Prediction

The integration of air curtain with moisture balance for supermarket model is necessary in order to assess the effect of reduced store relative humidity on display case energy requirements. So, thermodynamic analysis was used to simulate supermarket refrigeration/HVAC system using MATLAB software. For the simulated supermarket model described in this work with different types of refrigerated display cases, and located in a hot and humid weather such as Tampa, Florida, the annual average supermarket relative humidity was found to be 51.1%. This simulated store relative humidities were found to be in the range between 40% and 60% during the model year. The results show good agreement with previous model, and the experimental data validates the proposed model. The effect of indoor space conditions on supermarket energy consumption is studied. It is shown that for a 5% reduction in store relative humidity that the display case refrigeration load is reduced by 9.25%, and that results in total store energy load reduction of 4.84%. These results evaluated the integration of air curtain correlation for quick design calculation and for the simulation of different types of display cases within a supermarket model. These results, which are not generally known for typical supermarkets in hot and humid climates will now allow the designer of the supermarket to simply and quickly determine typical store relative humidity so that savings in display case operation and total store energy load are correctly estimated.

4.3 Recommendations for Future Research

In the first problem, Lithium bromide-water mixture was used as the working fluid for the solar absorption cooling system. This mixture shows quite good performance for Tampa, Florida weather condition. For future work, it is recommended to study the performance for different types of mixtures for optimum cooling performance. It is also recommended that the design specification for each component of the system i.e generator, evaporator, condenser, and absorber to be taken based on physical data. This will count for the number of tubes of the heat exchanger. The coefficient of performance will be varied with the overall heat transfer coefficient of the heat exchangers.

The effect of store relative humidity was investigated inside a typical supermarket in Tampa, Florida. The integration of store relative humidity with the display cases ($QL_{\text{display case}}$) within the moisture balance equation was highly effecting the energy consumption of the retail store. Finding new correlations for the other parameters of the moisture balance equation, i.e., QL_{produce}, QL_{meat}, and QL_{bakery}, gives more precise results for the energy consumed inside the retail store with changing the store relative humidity. It is also recommended to modify the model to be working for different weather conditions rather than hot and cold climate as Tampa, Florida. In addition, the model can be modified for different supermarket layouts.

References

[1] ASHRAE Handbook of Fundamentals, ASHRAE, Atlanta, USA, 1997.

[2] Wilbur, P.J., and Mitchell, C.E., "Solar absorption air conditioning alternatives", *Solar Energy*, vol. 17, no. 3, pp. 193-199, 1975.

[3] Li, Z.F., and Sumathy, K., "Simulation of a solar absorption air conditioning system", *Energy Conversion and Management*, vol. 42, no. 3, pp. 313-327, 2001.

[4] Li, Z.F., and Sumathy, K., "Experimental studies on a solar powered air conditioning system with partitioned hot water storage tank", *Solar Energy*, vol. 71, no. 5, pp. 285-297, 2001.

[5] Florides, G.A., Kalogirou, S.A., Tassou, S.A., and Wrobel, L.C., "Modelling and simulation of an absorption solar cooling system for Cyprus", *Solar Energy*, vol. 72, no. 1, pp. 43-51, 2002.

[6] Atmaca, I., and Yigit, A., "Simulation of solar-powered absorption cooling system", *Renewable Energy*, vol. 28, no. 8, pp.1277-1293, 2003.

[7] Florides, G.A., Kalogirou, S.A., Tassou, S.A., and Wrobel, L.C., "Design and construction of LiBr-water absorption machine", *Energy Conversion & Management*, vol. 44, no. 15, pp. 2483-2508, 2003.

[8] Assilzadeh, F., Kalogirou, S.A., Ali, Y., and Sopian, K., "Simulation and optimization of a LiBr solar absorption cooling system with evacuated tube collectors", *Renewable Energy*, vol. 30, no. 8, pp. 1143-1159, 2005.

[9] Mittal, V., Kasana, K.S., and Thakur, N.S., "Performance evaluation of solar absorption cooling system of Bahal (Hatyana)", *Journal of the Indian Institute of Science*, vol. 85, pp. 295-305, 2005.

[10] Sayegh, M.A., "The solar contribution to air conditioning systems for residential buildings", *Desalination*, vol. 209, vol. 1-3, pp. 171-176, 2007.

[11] Balghouthi, M., Chahbani, M.H., and Guizani, A., "Feasibility of solar absorption air condition in Tunisia", *Building and Environment*, vol. 43, no. 9, pp. 1459-1470, 2008.

[12] Mateus, T., and Oliveira, A.C., "Energy and economic analysis of an integrated solar absorption cooling and heating system in different building types and climates", *Applied Energy*, vol. 86, no. 6, pp. 949-957, 2009.

[13] Howell, R.H., and Adams, P.A., "Effects of indoor space conditions on refrigerated display case performance", Final report, ASHRAE-596 RP, 1991.

[14] Howell, R.H., "Effects of store relative humidity on refrigerated display case performance", *ASHRAE Transactions*, vol. 99, no. 1, pp. 667-678, 1993.

[15] Howell, R.H., "Calculation of humidity effects on energy requirements of refrigerated display cases", *ASHRAE Transactions*, vol. 99, no. 1, pp. 679-693, 1993.

[16] Tassou, S.A., and Datta, D., "Influence of supermarket environmental parameters on the frosting and defrosting of vertical multideck display cabinets", *ASHRAE Transactions*, vol. 105, no. 1, pp. 491-496, 1999.

[17] Orphelin, M., Marchio, D., and D'Alanzo, S.L., "Are there optimum temperature and humidity set points for supermarkets?", *ASHRAE Transactions*, vol. 105, no. 1, pp. 497-507, 1999.

[18] Rosario, L., and Howell, R.H., "Relative humidity and temperature measurement and predictions in supermarket", *ASHRAE Transactions*, vol. 107, no. 2, pp. 415-423, 2001.

[19] Kosar, D., and Dumitrescu, O., "Humidity effects on supermarket refrigerated case energy performance: a database review", *ASHRAE Transactions*, vol. 111, no. 1, pp. 1051-1060, 2005.

[20] Chen, Y.-G., and Yuan, X.-L., "Experimental study of the performance of single-band air curtains for a multi-deck refrigerated display cabinet", *Journal of Food Engineering*, vol. 69, no. 3, pp. 261-267, 2005.

[21] Smale, N.J., Moureh, J., and Cortella, G., "A review of numerical models of airflow in refrigerated food applications", *International Journal of Refrigeration*, vol. 29, no. 6, pp. 911-930, 2006.

[22] Getu, H.M., and Bansal, P.K., "Modeling and performance analyses of evaporators in frozen-food supermarket display cabinets at low temperatures", *International Journal of Refrigeration*, vol. 30, no. 7, pp. 1227-1243, 2007.

[23] Ge, Y.T., Tassou, S.A., and Hadawey, A., "Simulation of multi-deck medium temperature display cabinets with the integration of CFD and cooling coil models", *Applied Energy*, vol. 87, no. 10, pp. 3178-3188, 2010.

[24] Howell, R.H., Van, N.Q., and Smith, C.E., "Heat and moisture transfer through turbulent recirculated plane air curtains", *ASHRAE Transactions*, vol. 82, no. 2, pp. 191-205, 1976.

[25] Howell, R.H., and Shibata, M., "Optimum heat transfer through turbulent recirculated plane air curtains", *ASHRAE Transactions*, vol. 86, no. 1, pp. 188-200, 1980.

[26] Ge, Y.T., and Tassou, S.A., "Simulation of the performance of single jet air curtain for vertical refrigerated display cabinets", *Applied Thermal Engineering*, vol. 21, no. 2, pp. 201-219, 2001.

[27] Cui, J., and Wang, S., "Application of CFD in evaluation and energy-efficient design of air curtain for horizontal refrigerated display cases", *International Journal of Thermal Sciences*, vol. 43, no. 10, pp. 993-1002, 2004.

[28] Navaz, H.K., Amin, M., Dabiri, D., and Faramarzi, R., "Past, present, and future research toward air curtain performance optimization", *ASHRAE Transactions*, vol. 111, pp. 1083-1088, 2005.

[29] Ge, Y.T., and Cropper, R., "Performance simulation of refrigerated display cabinets operating with refrigerants R22 and R404A", *Applied Energy*, vol. 85, no. 8, pp. 694-707, 2008.

[30] Klein, S.A., Duffie, J.A., and Beckman, W.A., "Transient consideration of flat-plate solar collector", *Journal of Engineering for Power*, vol. 96, no. 2, pp.109-113, 1974.

[31] The 1991-2005 national solar radiation database, National Renewable Energy Labatory, Office of Energy and Renewable Energy, Alliance for Sustainable Energy, LLC.

[32] CHEMCAD. Version 6.1.2: Process Flow Sheet Simulator. Chemstations Inc.: Houston, 2008.

[33] Edwards, J.E., *Process modeling : Selection of thermodynamic methods*, P&I Design Ltd. Process Instrumentation Consultancy & Design, 2008.

[34] Peters, R., Korinth, C., and Keller, J.U., "Vapor-Liquid Equilibria in the System NH3 + H2O + LiBr. 2.Data Correlation", *Journal of Chemical & Engineering Data*, vol. 40, no. 4, pp. 775-783, 1995.

[35] Özkan, D., Agra, Ö., and Cetin, Ö. , "A comparison between refrigerants used in air conditioning", *Proceedings of Clima 2007 wellBeing Indoors*, pp. 1105-1114, REHVA World Congress, Finland, Helsinki, 2007.

[36] He, L.J., Tang, L.M., and Chen, G.M., "Performance prediction of refrigerant-DMF solutions in a single-stage solar-powered absorption refrigeration system at low generating temperatures", *Solar Energy*, vol. 83, no. 11, pp. 2029-2038, 2009.

[37] Kalogirou, S.A., "Solar thermal collectors and applications", *Progress in energy and Combustion Science*, vol. 30, no. 3, pp. 231–295, 2004.

[38] Gomri, R., "Investigation of the potential of application of single effect and multiple effect absorption cooling systems", *Energy Conversion & Management*, vol. 51, no. 8, pp. 1629-1636, 2010.

[39] Howell, R.H., Rosario, L., and Bula, A., "Effects of indoor relative humidity on refrigerated display case performance", *Proceedings of CLIMA 2000*, Brussells, Belgium, 1997.

[40] R.H. Howell, A. Bula, L. Rosario, Simulation of refrigerated display case performance in supermarkets. *Proceedings of the IASTED International Conference*, pp. 173-176, Banff, Canada, 1997.

[41] Weather data for 2000-2010, Tampa international airport, Weather warehouse, Weather Source, LLC.

[42] ASHRAE Handbook of Refrigeration, ASHRAE, Atlanta, USA, 2010.

[43] MATLAB. Version 7.6.0.324 (R2008a). The Mathworks Inc., Natick, Massachusetts, USA, 2008.

[44] *Cooling and heating load calculation manual*, prepared by ASHARE, Inc., U.S Department of Housing and Urban Development, Office of Policy Development and Research, H-2303 RP, USA, 1980.

[45] *Supermarket refrigeration assessment for the commonwealth electric company*, prepared by Foster-Miller, Inc., Final report, EPRI CU-7379, 2569-9 RP, 1991.

[46] *The assessment and evaluation of supermarket refrigeration in the state of New York*, Prepared by Foster-Miller, Inc., Final report, EPRI TR-100357, 2569-13 RP, 1992.

[47] Leach, M., Hale, E., Hirsch, A., and Torcellini, P., "Grocery Store 50% Energy Savings", Technical report, NREL/TP-550-46101, 2009.

[48] Stoecker, W.F., *Design of thermal systems*, 2nd ed., McGraw-Hill, Inc., USA, 1980.

[49] Stoecker, W.F., and Jones, J.W., *Refrigeration and air conditioning*, 2nd ed., McGraw-Hill, Inc., USA, 1982.

[50] Bell, A.A., *HVAC : Equations, Data, and Rules of thumb*. McGraw-Hill, Inc., USA, 2000.

[51] Sauer, H.J., Howell, R.H., and Coad, W.J., *Principles of heating, ventilating, and air conditioning : A textbook with design data based on the 2001 ASHRAE Handbook-Fundamentals*, American Society of Heating, Refrigerating and Air-Conditioning Engineers, Inc., Atlanta, USA, 2001.

[52] McQuiston, F.C., Parker, J.D., and Spitler, J.D., *Heating, ventilating, and air conditioning: analysis and design*, 6th ed., John Wiley & Sons, Inc., USA, 2005.

Appendices

Appendix A: MATLAB Code for Modeling of Supermarket Refrigeration/HVAC System

A.1 Main M-file

```
%main.m
close all
clear all
clc
%given
CFMspace=30000; %cfm (4.16m^3/s)
NP_max=180; %(maximum number of people in the store)
%operations time
time=1:24;
%Specified operation month by input the number of the month (1-12)
month=1:12;
%people occupancy in supermarket (NP)
NP=[0.17*NP_max 0.17*NP_max 0.17*NP_max 0.17*NP_max 0.17*NP_max
0.17*NP_max 0.17*NP_max 0.33*NP_max 0.50*NP_max 0.50*NP_max 0.50*NP_max
1.00*NP_max 1.00*NP_max 1.00*NP_max 0.50*NP_max 0.50*NP_max 0.50*NP_max
0.50*NP_max 1.00*NP_max 1.00*NP_max 1.00*NP_max 0.67*NP_max 0.67*NP_max
0.50*NP_max];
tspace=75; %indoor space condition temperature in F, (24C)
%Plot the schedule of people occupancy in supermarket
bar(time,NP,0.5,'r')
set(gca,'XTick',1:2:24)
set(gca,'XTickLabel',{'1','3','5','7','9','11','13','15','17','19','21'
,'23'})
axis([0 25 0 200])
xlabel('Hour')
```

Appendix A: (Continued)

```
ylabel('Number of people')
figure
delP_build=4.02; %pressure difference of building
t_supply=55; %supply temperature in F, (13C)
fi_supply=95; %supply relative humidity of air 95%
w_supply=solve_w(t_supply,fi_supply/100); %calculate supply humidity
ratio
S=str2mat('January','February','March','April','May','June','July','Aug
ust','September','October','November','December');
%model
for j=1:length(month)
%call for outdoor temperature (F) and relative humidity (%) for
specified month
[t_outside,fi_outside]=data(j);
%Plot temperature and relative humidity profiles for all months for
averaged years (2000-2010) in Tampa,FL
subplot(3,4,j)
plot(time,t_outside,'r-o',time,fi_outside,'b-+')
axis([0 25 40 90])
xlabel('Hour')
ylabel('Temperature (F) and relative humidity (%)')
title([S(j,:)])
legend('Temperature (F)','Relative humidity (%)')
 %calculate the humidity ratio for given outdoor temperature (F) and
relative humidity
for k=1:length(t_outside)
w_outside(k)=solve_w(t_outside(k),fi_outside(k)/100); % tempearture in
```

Appendix A: (Continued)

```
F and fi in NaN
end
for i=1:length(time)
CFMinfl(i)=(44.5*NP(i)-0.095*(NP(i))^2+1e-4*(NP(i))^3)*delP_build;
QLpeople(i)=255*NP(i);
QLproduce(i)=1400; %BTU/hr (constant for 24 hours)
if (i>=5 && i<10)
QLmeat(i)=1400; %BTU/hr (from 5am to 10am)
else
QLmeat(i)=0;
end
if (i>=5 && i<22)
QLbakery(i)=12000; %BTU/hr (from 5am to 10pm)
else
QLbakery(i)=0;
End
QLdisplay(i)=17280+68400+34200; %display cases latent loads (Btu/hr)
total1(i)=QLpeople(i)+QLproduce(i)+QLmeat(i)+QLbakery(i)-QLdisplay(i);
total2(i)=QLpeople(i)+QLproduce(i)+QLmeat(i)+QLbakery(i);
w_space(j,i)=solve_w_space(total1(i),CFMinfl(i),CFMspace,w_supply,w_out
side(i));
w_space_new(j,i)=solve_w_spacenew(total2(i),CFMinfl(i),CFMspace,tspace,
w_supply,w_outside(i));
fi_space(j,i)=solve_fi(w_space(j,i),tspace);
fi_space_new(j,i)=solve_fi(w_space_new(j,i),tspace);
fi_space_month(j,i)=fi_space(j,i); %row is the month (j) , column is
Hour (i)
```

Appendix A: (Continued)

```
fi_space_month_new(j,i)=fi_space_new(j,i);
end
end
%plot relative humidity for each month for both models
figure
for j=1:length(month)
subplot(3,4,j)
%Y=[fi_space_month(j,:)'.*100 fi_space_month_new(j,:)'.*100];
Y=[fi_space_month_new(j,:)'.*100];
bar(Y,0.5)
axis([0 25 0 80])
xlabel('Hour')
ylabel('relative humidity (%)')
title([S(j,:)])
%legend('old','new')
end
%average relative humidity for each month
average=mean(fi_space_month')*100;
average_new=mean(fi_space_month_new')*100;
%average monthly relative humidity inside store for old model
(original)
average_rh=[46.3 47.2 48 48.6 52 55 58.2 58.2 58.2 47.9 47.5 46.8];
%Comparison plot the monthly averaged space relative humidity for old
and new models
figure
plot(month,average_rh,'-^r')
hold on
```

Appendix A: (Continued)

```
plot(month,average_new,'-ob')
set(gca,'xtick',1:1:12)
set(gca,'xticklabel',str2mat('Jan','Feb','Mar','Apr','May','Jun','Jul',
'Aug','Sep','Oct','Nov','Dec'))
axis([0 13 30 70])
xlabel('Months')
ylabel('Relative humidity (%)')
%title('Comparison of relative humidity for old and new models')
legend('Model [39]','Current model')
%average monthly relative humidity inside store for (experimental)
rh_exp_max=[45.56 45.27 30.78 50.55 51.94 56.21 59.13 58.05 0 58.03
41.68 42.26];
rh_exp_avg=[42.58 41.24 27.23 47.80 49.45 52.61 54.75 52.85 51.51 54.48
39.83 40.24];
rh_exp_min=[37.54 38.41 24.45 41.43 42.94 45.74 47.38 45.08 0 47.47
37.42 36.75];
%Comparison plot the monthly averaged space relative humidity for
experimental and new model
figure
plot(month,rh_exp_max,'^k')
hold on
plot(month,rh_exp_avg,'-or')
plot(month,rh_exp_min,'db')
plot(month,average_new,'--sb')
set(gca,'xtick',1:1:12)
set(gca,'xticklabel',str2mat('Jan','Feb','Mar','Apr','May','Jun','Jul',
'Aug','Sep','Oct','Nov','Dec'))
```

Appendix A: (Continued)

```
axis([0 13 10 70])
xlabel('Months')
ylabel('Relative humidity (%)')
%title('Comparison of relative humidity for old and new models')
legend('EXP RHmax','EXP RHavg','EXP RHmin','Current model')
%Experimental store relative humidity (%) for display cases for 24
hours
exp_rh=[35 34 33 33 34 33 36 37 39 40 40 40 40 40 41 40 39 39 39 39 36
34 34 37];
%Comparison plot the hourly averaged space relative humidity for
experimental data and current models for month 12
figure
plot(time,exp_rh,'^r')
hold on
plot(time,fi_space_month_new(12,:).*100,'-ob')
set(gca,'XTick',1:2:24)
set(gca,'XTickLabel',{'1','3','5','7','9','11','13','15','17','19','21'
,'23'})
axis([0 25 20 60])
xlabel('Hour')
ylabel('Relative humidity (%)')
%title('Comparison of relative humidity for experimental and current
model for Month 12')
legend('Experimental data [22]','Current model')
%average hourly relative humidity inside store for Month 1 for old
model (original)
time_old=[1 4 8 10 12 16 19 22 24];
```

Appendix A: (Continued)

```
rh_month1=[43 45 45 46 44 48 42 47 43];
%rh_month1=[48 47 46 45 51.5 51.5 51 51 50.5 50.5 45 44 43 42 49.5 48
49 39.5 40 40 40 47 46 48];
%Comparison plot the hourly averaged space relative humidity for old
and new models for Month 1
figure
plot(time_old,rh_month1,'^r')
hold on
plot(time,fi_space_month_new(1,:).*100,'-ob')
set(gca,'XTick',1:2:24)
set(gca,'XTickLabel',{'1','3','5','7','9','11','13','15','17','19','21'
,'23'})
axis([0 25 20 70])
xlabel('Hour')
ylabel('Relative humidity (%)')
%title('Comparison of relative humidity for old and new models for
Month 1')
legend('Model [39]','Current model')
%average hourly relative humidity inside store for Month 8 for old
model (original)
time_old=[1 4 8 10 12 16 19 22 24];
rh_month8=[51.5 52.5 58 66 65 61 66 59.5 60];
%rh_month8=[51.5 51.5 52.5 52.5 57 58.5 64.5 67 69.5 70.5 58 56.5 56 55
62.5 61 61 52.5 52.5 52.5 51.5 59.5 59.5 60];
%Comparison plot the hourly averaged space relative humidity for old
and new models for Month 1
figure
```

Appendix A: (Continued)

```
plot(time_old,rh_month8,'^r')
hold on
plot(time,fi_space_month_new(8,:).*100,'-ob')
set(gca,'XTick',1:2:24)
set(gca,'XTickLabel',{'1','3','5','7','9','11','13','15','17','19','21'
,'23'})
axis([0 25 20 90])
xlabel('Hour')
ylabel('Relative humidity (%)')
%title('Comparison of relative humidity for old and new models for
Month 8')
legend('Model [39]','Current model')
%annual average of the monthly averaged relative humidity
annual_average=mean(average)
annual_average_new=mean(average_new)
```

A.2 Tampa Climate Data M-file

```
% data.m
function [t,fi]=data(month)
% Hourly temperature (F) and relative humidity (%) for Tampa,FL
averaged (2000-2010)
if month == 1
t=[56.839296 56.169013 55.556598 54.900293 54.336911 53.895601
53.601173 53.526237 53.962757 56.965689 60.381681 63.185924 65.193861
66.626393 67.472278 67.465357 66.908768 65.574194 62.926979 60.889150
59.647214 58.722348 58.146628 57.430714];
```

Appendix A: (Continued)

```
fi=[80.879765 81.827761 82.554252 83.252199 83.555230 83.741935
83.520039 83.311828 82.492669 77.178886 70.297361 64.354839 60.364614
57.604106 56.194428 55.190029 56.346823 58.909091 64.785924 70.070381
73.354839 75.660229 77.410557 79.208798];
elseif month == 2
t=[58.917419 58.274029 57.630329 57.098095 56.673360 56.249214
56.057564 56.031134 56.986274 60.077239 63.113099 65.647450 67.545097
68.867667 69.361487 69.506538 69.182871 68.051019 66.005804 63.493014
62.028161 61.031785 60.437293 59.814514];
fi=[79.428505 80.622180 81.798762 82.657816 82.858250 83.454633
83.209003 82.704442 80.916592 74.310233 67.427004 62.347618 58.981295
56.148679 55.366099 54.737909 55.673197 57.427788 61.662313 67.455217
71.809287 74.484662 75.905732 77.531456];
elseif month == 3
t=[64.341935 63.590029 62.807918 62.262272 61.691799 61.338104
61.207380 61.048974 62.678006 65.580059 68.627273 70.885924
72.634018 73.855718 74.526344 74.828739 74.503597 73.507918 71.797654
69.454565 67.723167 66.530205 65.904985 65.280059];
fi=[76.612903 77.762463 79.416422 80.777622 81.781720 82.347019
82.287879 82.460411 79.137830 72.888563 65.615836 60.624633 57.281525
54.527859 53.336168 52.850440 53.504301 55.592375 58.782991 63.701369
68.290323 71.909091 73.715543 75.313783];
elseif month == 4
t=[68.783636 68.003636 67.178788 66.531609 65.847879 65.333030
65.053939 64.855758 65.981818 69.153187 72.237576 74.593030 76.446667
78.013333 78.986970 79.575758 79.612121 79.078788 77.926364 75.855455
73.204848 71.357273 70.296667 69.651014];
```

Appendix A: (Continued)

```
fi=[73.387879 75.015152 76.678788 78.695925 79.951515 81.021212
81.700000 81.893939 80.066667 72.940857 65.157576 59.569697 55.648485
52.484848 50.357576 49.181818 49.087879 49.981818 52.160606 56.090909
61.009091 66.403030 69.348485 71.192372];
elseif month == 5
t=[74.928446 74.193109 73.486510 72.841935 72.228446 71.821212
71.424340 71.338710 73.190440 75.965924 78.462564 80.555288 82.362258
83.775357 84.960117 85.650147 85.754330 85.156012 83.951613 82.265396
79.858935 77.921994 76.767155 75.882698];
fi=[74.401760 76.106256 77.941349 79.733138 81.369501 82.537732
83.454545 83.803519 80.499609 73.719746 67.307716 61.812805 57.907625
54.854154 51.794721 50.527859 50.285337 51.592375 53.706745 56.703812
61.271554 66.695015 70.190616 72.580645];
elseif month == 6
t=[78.434577 77.920522 77.363939 76.912121 76.538182 76.390606
76.153939 76.356970 78.078182 80.236970 82.287743 83.993166
85.419739 86.550303 86.874242 87.394242 87.163636 86.436061 85.170000
83.757576 81.774807 80.040909 79.467879 78.917983];
fi=[79.744932 81.119854 82.251515 83.848485 84.784013 85.387879
86.071645 85.893939 83.012121 78.333333 73.236573 68.915674 64.969488
62.136364 61.360606 60.157576 60.463636 61.690909 64.154545 66.839394
70.678474 75.221212 77.139812 78.885162];
elseif month == 7
t=[79.617595 79.194721 78.756970 78.369912 78.016051 77.897595
77.802522 77.831085 79.216716 81.296667 83.116256 84.585711 85.661848
86.400587 87.034897 86.931271 86.723167 86.082698 85.172141 83.936364
82.631085 81.216129 80.581525 80.039883];
```

Appendix A: (Continued)

```
fi=[80.451613 81.806452 83.056989 84.388856 85.502737 85.928446
86.118182 86.378299 84.052786 79.324242 75.203324 71.731419 68.896383
66.903324 65.070381 64.390323 64.545455 65.909091 67.501466 70.219941
72.923754 76.117302 77.829912 79.401760];
elseif month == 8
t=[79.853666 79.438123 79.013196 78.514370 78.220528 77.960704
77.805279 77.769824 78.718524 81.111378 83.233969 84.907038 85.948788
86.851026 87.202170 87.270459 87.191750 86.789189 85.776246 84.284751
82.606452 81.460117 80.705572 80.263343];
fi=[81.489736 82.478006 83.604106 85.029326 86.190616 86.923754
87.351906 87.332063 85.949267 80.991691 75.802444 71.856305 69.062561
66.868035 65.316227 65.066667 65.034506 65.742131 67.278592 70.284457
73.806452 76.909091 79.126100 80.234604];
elseif month == 9
t=[78.298182 77.825152 77.261672 76.819216 76.439613 76.150000
75.999091 75.893511 76.343939 78.784420 81.278485 83.286970
84.937367 85.933030 86.741515 87.056364 86.888401 86.183762 84.984545
83.180909 80.982194 79.987900 79.279969 78.727576];
fi=[81.403030 82.693939 84.267189 85.481923 86.504702 87.221212
87.396970 87.605538 86.778788 81.482445 75.118182 70.257576 66.217973
63.300000 61.427273 60.672727 60.864890 61.934796 64.115152 67.821212
72.796552 75.656113 77.664890 79.366667];
elseif month == 10
t=[73.074927 72.263675 71.594064 70.947952 70.403069 70.055142
69.816882 69.690792 69.888671 72.544839 75.804454 78.523063 80.636843
81.917234 82.740313 83.145637 83.200860 82.391271 80.854076 78.481565
76.491281 75.199531 74.392405 73.649218];
```

Appendix A: (Continued)

```
fi=[77.935679 79.780743 81.179391 82.374558 83.533529 84.249169
84.491202 84.612610 84.093842 78.773021 71.175785 64.893976 60.070772
57.219355 55.482307 54.148953 53.815957 55.049267 58.194428 63.174032
68.167351 71.943011 74.392278 76.217400];
elseif month == 11
t=[64.736729 63.867273 63.185455 62.612957 62.166667 61.873030
61.672424 61.640084 63.337273 66.920000 70.384556 72.873636 74.688182
75.729478 76.066625 76.100303 75.357273 73.695789 70.936061 69.068422
67.882424 66.916364 66.145977 65.344692];
fi=[78.343365 80.027273 81.378788 82.298224 83.087879 83.375758
83.475758 83.048589 80.009091 72.857576 65.392163 60.772727 57.281818
55.232393 54.293939 53.906061 55.286729 58.381714 64.357576 68.968652
72.151515 74.427273 76.129781 77.261129];
elseif month == 12
t=[59.506940 58.854751 58.069355 57.630332 57.152364 56.789335
56.667380 56.621994 57.135327 59.902561 62.989736 65.618182
67.589257 68.779179 69.518397 69.697243 69.159756 67.615357 65.169892
63.501760 62.384457 61.514858 60.703284 60.048573];
fi=[80.064223 80.994330 81.860508 82.613783 83.263033 83.479277
83.324633 83.105572 81.550342 75.967253 69.495601 64.672825 60.962170
58.762463 57.350342 56.649756 57.908895 60.498729 66.042522 70.260997
73.143695 75.525024 77.605474 78.668328];
%fi=[69 69 69 69 69 86 72 73 72 70 69 69 69 68 77 70 73 89 75 77 84 70
38 71]; % fi of Auckland, New Zealand December 2004
end
```

Appendix A: (Continued)

A.3 Solving for Relative Humidity M-file

```
% solve_fi.m
function fi=solve_fi(w,t)
% Given: humidity ratio (w), dry bulb temp (t in F), pressure
T=t+459.67; %R
P=14.696; %psia (pressure at sea level)
c8=-1.0440397e+04;
c9=-1.129465e+01;
c10=-2.7022355e-2;
c11=1.2890360e-05;
c12=-2.4870681e-09;
c13=6.5459673e+00;
Pws=exp(c8/T+c9+c10*T+c11*T^2+c12*T^3+c13*log(T)); %Psia
Pw=w*P/(0.621945+w);
fi=Pw/Pws;
```

A.4 Solving for Humidity Ratio M-file

```
% solve_w.m
function w=solve_w(t,fi)
% Given: dry bulb temp (t in F), relative humidity (fi), pressure
T=t+459.67; %R
P=14.696; %psia (pressure at sea level)
c8=-1.0440397e+04;
c9=-1.129465e+01;
c10=-2.7022355e-2;
c11=1.2890360e-05;
c12=-2.4870681e-09;
```

Appendix A: (Continued)

```
c13=6.5459673e+00;
Pws=exp(c8/T+c9+c10*T+c11*T^2+c12*T^3+c13*log(T)); %Psia
Pw=fi*Pws; %Psia
w=0.621945*Pw/(P-Pw);
h=0.24*t+w*(1061+0.444*t); %Btu/lb
```

A.5 Solving for Store Humidity Ratio of Old Model M-file

```
% solve_w_space.m
function w=solve_w_space(total1,CFMinfl,CFMspace,w_supply,w_outside)
syms w_space
QLspace=4840*CFMspace*(w_space-w_supply);
QLinfil=4840*CFMinfl*(w_space-w_outside);
Total=total1-QLspace-QLinfil;
w=double(solve(Total,w_space));
```

A.6 Solving for Store Humidity Ratio of New Model M-file

```
% solve_w_spacenew.m
function
w=solve_w_spacenew(total2,CFMinfl,CFMspace,tspace,w_supply,w_outside)
syms w_space
t=(tspace-32)*5/9; % space temperature in C (tspace = 75F)
%s stands for single display case
%m stands for multi decks display case
%c stands for closed door display case
%inlet air curtain temperature in K
Tin_s=275.15;
```

Appendix A: (Continued)

```
Tin_m=273.15;
Tin_c=268.75;
%difference of display case temperature - inlet air curtain temperature
deltaT_s=2.4;
deltaT_m=3;
deltaT_c=2.4;
% air curtain mass flow rate (ma=ro*v*A) where A = width*thickness
ma_s=1.2*0.5588*0.1016;
ma_m=1.2*1.325*0.114;
ma_c=1.2*0.675*0.0613;
%correlation's constants for heat transfer across the air curtain
c1=-0.180;
c2=303.180;
c3=-0.781;
c4=216.309;
c5=-0.448;
c6=509.975;
h=1.0*t+w_space*(2501.3+1.86*t); % enthalpy of the space in kJ/kg
Qsingle=(c1*h^2+c2*h+c3*(Tin_s+deltaT_s)^2+c4*(Tin_s+deltaT_s)+c5*h*(Ti
n_s+deltaT_s)+c6)*ma_s;
Qmulti=(c1*h^2+c2*h+c3*(Tin_m+deltaT_m)^2+c4*(Tin_m+deltaT_m)+c5*h*(Tin
_m+deltaT_m)+c6)*ma_m;
Qclosed=(c1*h^2+c2*h+c3*(Tin_c+deltaT_c)^2+c4*(Tin_c+deltaT_c)+c5*h*(Ti
n_c+deltaT_c)+c6)*ma_c;
QLdisplay=(0.12*73*Qsingle+0.19*73*Qmulti+0.19*91*Qclosed)*3.412;
%total latent heat across all display cases
QLspace=4840*CFMspace*(w_space-w_supply); %Btu/hr
```

Appendix A: (Continued)

```
QLinfil=4840*CFMinfl*(w_space-w_outside); %Btu/hr

Total=total2-QLspace-QLinfil-QLdisplay;

solve_w=double(solve(Total,w_space));

%because we have two solutions for relative humidity, we choose the
value that is less than 1

for i=1:length(solve_w)

if (solve_w(i)>0 && solve_w(i)<1)

w=solve_w(i);

end

end
```

About the Author

Ammar Mohammad Khalil Bahman was born in Birmingham, United Kingdom, on Nov. 29, 1984. The author received his Bachelor's degree in Mechanical Engineering in 2006 from Kuwait University, College of Engineering and Petroleum. He received his Master degree in Mechanical Engineering under the supervision of Professor Walid Chakroun in 2009 from Kuwait University, College of Engineering and Petroleum. In addition, he worked for Kuwait Oil Company as a mechanical maintenance engineer from Nov. 2007 to Feb. 2008. Then, he worked as a teaching assistant for the Mechanical Engineering Department in the College of Engineering and Petroleum, Kuwait University, from Mar. 2008 to Aug. 2009. He joined the Public Authority for Applied Education and Training (PAAET), Kuwait, as a teaching assistant in Aug. 2009. The author is a member of the American Society of Mechanical Engineers (ASME), and an associate member of the American Society for Heating, Refrigerating and Air Conditioning Engineers (ASHRAE) since 2004.